First Multi-Isotopic (Pb-Nd-Sr-Zn-Cu-Fe) Characterisation of Dust Reference Materials (ATD and BCR-723): A Multi-Column Chromatographic Method Optimised to Trace Mineral and Anthropogenic Dust Sources

Vanderstraeten, Aubry; Bonneville, Steeve; Gili, Stefania; de Jong, Jeroen; Debouge, Wendy; Claeys, Philippe; Mattielli, Nadine

Published in:
Geostandards and Geoanalytical Research

Publication date:
2020

Document Version:
Accepted author manuscript

First Multi-Isotopic (Pb-Nd-Sr-Zn-Cu-Fe) Characterisation of Dust Reference Materials (ATD and BCR-723): A Multi-Column Chromatographic Method Optimised to Trace Mineral and Anthropogenic Dust Sources

Aubry Vanderstraeten (1)*, Steeve Bonneville (2), Stefania Gili (1), Jeroen de Jong (1), Wendy Debouge (1), Philippe Claeys (3) and Nadine Mattielli (1)*

(1) Laboratoire G-Time, De'partement G'eosciences, Environnement et Socie't'e (DGES), Universit'e Libre de Bruxelles (ULB), Av. F. Roosevelt 50 (CP160/02), Brussels,1050, Belgium
(2) Biogeochimie et Modelisation du Systeme Terre (BGeOsys), De'partement Ge'osciences, Environnement et Soci'ete' (DGES), Universite' Libre de Bruxelles (ULB), Av. F. Roosevelt 50 (CP160/02), Brussels,1050, Belgium
(3) Analytical, Environmental and Geo-Chemistry, Earth System Science, Vrije Universiteit Brussels (VUB), Brussels,1050, Belgium
* Corresponding author. e-mail: auvdstra@ulb.ac.be; nmattiel@ulb.ac.be

Atmospheric dust is an integral component of the Earth system with major implications for the climate, biosphere and public health. In this context, identifying and quantifying the provenance and the processes generating the various types of dust found in the atmosphere is paramount. Isotopic signatures of Pb, Nd, Sr, Zn, Cu and Fe are commonly used as sensitive geochemical tracers. However, their combined use is limited by the lack of (a) a dedicated chromatographic protocol to separate the six elements of interest for low-mass samples and (b) specific reference materials for dust. Indeed, our work shows that USGS rock reference materials BHVO-2, AGV-2 and G-2 are not applicable as substitute reference materials for dust. We characterised the isotopic signatures of these six elements in dust reference materials ATD and BCR-723, representatives of natural and urban environments, respectively. To achieve this, we developed a specific procedure for dust, applicable in the 4–25 mg mass range, to separate the six elements using a multi-column ion-exchange chromatographic method and MC-ICP-MS measurements.

Keywords: mineral and anthropogenic dust, Pb, Nd, Sr, Zn, Cu and Fe isotopes, ATD, BCR-723, dust reference materials, chromatography, geochemical tracers.

Atmospheric dust plays a crucial role in the Earth system as it influences several important environmental compartments on Earth's surface. First, dust affects the radiative balance of the Earth by either absorbing or reflecting solar energy flux depending on its chemical composition, mineralogy, grain-size and vertical distribution in the atmosphere (Perlwitz *et al.* 2001, Mahowald *et al.* 2014). For instance, dust falls on Greenland ice sheet can alter the ice albedo and amplify large-scale melting (e.g., Wientjes *et al.* 2011). Second, dust deposition over remote portion of the global ocean (and also on Amazonian forest) can strongly stimulate primary productivity by providing to those biomes essential bio-limiting elements such as iron and/or phosphorus (Rizzolo *et al.* 2017). This dust-biosphere connection may represent an important feedback loop on Earth's climate through the removal of CO_2 from the atmosphere (Martin 1990). Third, dust is also an efficient, long-ranged dispersion agent of anthropogenic pollutants, which is of major concerns for public health in the ever-growing, densely populated areas (Wang *et al.* 2018). The above-mentioned list of dust impacts on climate, biogeochemistry and public health – far from being exhaustive – clearly highlights the need for a better understanding of dust sources, transport mechanisms and deposition processes. Among those challenges, the most pressing issue is to develop robust and versatile methods able to quantitatively trace the sources of dust.

Developed over the last two decades, a promising direction is to apply geochemical tracers, such as isotopes to relate aeolian dust deposits – both recent and ancient – to their contemporaneous source area(s) or anthropogenic generating process(es). Radiogenic isotopes (i.e., Pb, Nd and Sr) are considered conservative; that is, they do not fractionate during dust atmospheric transport and fingerprint the dust precursor. Often associated together in studies tracing dust, Nd and Sr isotopes are widely applied to distinguish dust source region at the continent-scale to separate local sources (e.g., Scheuvens *et al.* 2013) or to distinguish the contribution of various continents (e.g., Basile *et al.* 1997). Neodymium and Sr are also largely used to identify dust inputs in geological records such as ice, peat, lacustrine and marine sediment cores (e.g., Delmonte *et al.* 2010, Le Roux *et al.* 2012). While Pb is a good complement for tracing natural sources, it is mainly a long-standing tracer of anthropogenic activities from mining, cupellation and ore smelting in roman times to modern automobile traffic and coal burning (Grousset and Biscaye 2005, Komárek *et al.* 2008).

In contrast to Sr, Nd and Pb, non-traditional stable isotopic systems such as Zn, Cu and Fe will fractionate during specific natural (e.g., sorption, complexation, redox transformations) or industrial (e.g., smelting and distillation) processes. The mass fractionation of these metal isotopes is more and more used to distinguish specific natural (bio)geochemical (Cloquet *et al.* 2008, Weiss *et al.* 2008, Wiederhold 2015) or anthropogenic processes (Flament *et al.* 2008, Mattielli *et al.* 2009). Recent studies explored Zn and Cu combined with Pb isotopes as tracers of the multiple sources of anthropogenic dust in urban environments. It allowed for instance to quantify the contribution of exhaust (petrol, diesel), non-exhaust (tyres, brakes) automobile emissions, waste incinerator, industrial emissions, biomass burning or even construction activities (cement) (Cloquet *et al.* 2006, Gioia *et al.* 2008, Ochoa Gonzalez *et al.* 2016, Dong *et al.* 2017, Souto-Oliveira *et al.* 2018). These studies highlight the interest of a multi-isotopic approach to distinguish and identify specific dust generation processes and derive their geographical origin in a given local urban context.

So far, the applicability of radiogenic and stable isotopes to dust is limited because of the low mass (typically in the mg range) of atmospheric samples and the destructive analytical procedure. In this context, there is a clear need for an optimised method to sequentially separate these six elements (Pb, Nd, Sr, Zn, Cu, Fe) together in a given atmospheric sample from a single aliquot. In the most recent publications that combine at least three isotopic systems (e.g., Pin *et al.* 2014, Sossi *et al.* 2015, Retzmann *et al.* 2017), the chromatographic techniques are based on rock reference materials and tend to reduce the number of columns, the handling, reagent consumption and the total analytical blank. In the context of dust, the sample matrix (e.g., mineralogy, major element and organic contents) is a key factor, which can be very different from rock samples and can vary greatly between natural and anthropogenic dust samples. Those discrepancies in matrix components can induce large peak shifts during the chromatographic procedure and affect element separation.

Here, we aimed at developing a versatile method based on a multi-column scheme adapted for optimal recovery whatever the dust origin is. From an analytical point of view, the challenge lies in the capacity of this method to provide low procedural blank and optimal yields for a large variety of dust type while giving accurate, precise and reproducible results for all six isotopic systems, all this from a unique, low-mass sample (or aliquot). In order to validate our multi-column scheme, we used three USGS rock reference materials (BVHO-2, AGV-2 and G-2), two new proposed dust reference materials (Arizona Test Dust – ATD – and IRMM BCR-723) plus three natural dust samples from the Gobi, Patagonia and Sahara deserts. A major hurdle to the application of the multi-isotopic approach for dust is the lack of reference materials. Here, we carried out an in-depth isotopic characterisation of ATD and BCR-723 that are proposed as new reference materials for natural-like and urban-like environments, respectively.

Experimental methods

Reagents, rocks, dust reference materials and dust samples

The sample preparation and chemistry were performed under a laminar flow hood (Class 100) in a Class 1000 laboratory. The main reagents – 6 and 8 mol l^{-1} HCl, 14 mol l^{-1} HNO_3, 23 mol l^{-1} HF and 47% *m*/*m* HBr (pro-analis, Merck®, Darmstadt, Germany) – were systematically purified via distillation and sub-boiling (at 68 °C, Analab purification system, Bischheim, France) before use. High-purity water (Milli-Q, 18.2 MΩ cm), 12 mol l^{-1} HCl (Ultrapur) and 30% H_2O_2 (~ 8.8% *m*/*m* – Suprapur, VWR®, Oud-Heverlee, Belgium) were also used. All analytical procedures were performed under the cleanest conditions with acid-cleaned Savillex® (Eden Prairie, MN, USA) or PTFE vials, acid-cleaned uncoloured tips and powder-free gloves to prevent any contamination (Gar_con *et al.* 2017).

Five reference materials (Table 1) were used in our study: (a) a basalt (USGS BVHO-2), (b) an andesitic lava (USGS AGV-2), (c) a granite (USGS G-2), (d) a natural-like dust (Nominal 0–3 μm Arizona Test Dust 'ATD' from Powder Technology Inc.) and (e) a road dust (IRMM BCR-723). The

Table 1.
Provenance, general characterisation and analyte mass fraction of rock and dust materials used in this study

RM/ Natural samples	Type	Issuing organisation	Provenance	L. Ign [a]	Pb	Nd	Sr	Zn	Cu	Fe
				% *m*/*m*	µg g^{-1} [b]					% [b]
BHVO-2	Basalt	USGS	Halemaumau Crater, Hawaii	-	1.7	25	389	103	127	8.6
AGV-2	Andesite	USGS	Guano Valley, Oregon	-	13	30	658	86	53	4.6
G-2	Granite	USGS	Sullivan quarry, Rhode Island	-	30	55	478	86	11	2.7
ATD nominal 0–3 µm	Natural aerosol	Powder Technology inc	Salt River Valley, Arizona	1.1	33	32	278	130	45	3.0
BCR-723	Road dust	IRMM	Tanzenberg tunnel – Styria, Austria	21.1	841	14	211	1552	216	3.0
Sahara	Dust precursor	In-house sample	Bou Arfa area, SE Eastern Morocco	0.8	3.0	4.4	54	7.6	2.8	0.2
Patagonia	Dust precursor	In-house sample	Col De La Picada, area of Calbuco volcano, Chile	0.2	3.9	10	371	71	39	3.2
Gobi desert	Dust precursor	In-house sample	Dulaan Uul camp area, Dornogovi, SE Mongolia	2.6	21	21	241	45	16	1.1

[a] L. Ign stands for loss on ignition (i.e., weight loss after ashing at 450 °C for 4 h) giving an estimate of the organic matter content.
[b] Data for USGS rocks are certified values; other data were obtained during the present study.

three well-characterised certified USGS rocks were selected here as natural proxies with contrasted matrices to validate our analytical method. ATD is a natural-like aerosol material collected in the Salt River Valley, Arizona, and is currently under assessment to become a consensus reference dust material (Shelley *et al.* 2015). BCR-723 is a road dust material collected from the ceiling of the Tanzemberg Tunnel (Styria, Austria) referenced so far for platinum-group element studies but not for its entire elemental composition or isotopic signature.

In addition, we used natural dust precursors from the Patagonia, Gobi and Sahara deserts (Table 1), hence covering three main dust source regions at the global scale. The idea was to validate our elution scheme with natural dust samples (hereafter referred to as 'natural dust samples') exhibiting various mineralogy and elemental contents.

Dissolution

Between 25 and 150 mg for USGS reference materials and 4–25 mg for ATD, BCR-723 and natural dust samples were carefully weighed (Sartorius balance model CPA225D). BHVO-2 and AGV-2 were dissolved in a 6-ml squared-body Savillex® beaker with 3 ml 14 mol l^{-1} HNO_3 and 1 ml 23 mol l^{-1} HF on a hot plate at 120 °C for 48 h. Samples were dried down on a hot plate at 90 °C before addition of 2 ml 12 mol l^{-1} HCl and re-dissolved for 24 h at 120 °C until the solution was clear and without any residue. Lastly, the solutions were dried down again before their use in the chromatographic procedure.

As granite G-2 contains accessory minerals resistant to the initial HF-HNO_3 dissolution, this reference material underwent an extra digestion step in a PAAR® high-pressure PTFE dissolution vessel (PAAR). Briefly, following the HF-HNO_3 dissolution step, the supernatant and the solid residues were evaporated to dryness separately. The solid residues were then transferred into a PAAR vessel with 2 ml 14 mol l^{-1} HNO_3 and 2 ml 23 mol l^{-1} HF and placed in an oven at 180 °C for 48 h. The PAAR vessel liquid content and the dried-out supernatant were re-homogenised and then again dried and re-dissolved in 2 ml 6 mol l^{-1} HCl on a hot plate for 24 h at 120 °C. The transparent solution was evaporated to dryness before being used in the chromatographic procedure.

ATD, BCR-723 and natural dust samples contain significant amounts of organic matter (the mass difference, due to the loss on ignition, is reported in Table 1 and gives

an estimation of the organic matter content) that can affect the elution rate during chromatography and also compromise the isotopic measurements. Thus, these samples were placed in slightly open ceramic crucibles in a muffle furnace at 450 °C for a minimum of 4 h until a white ash was obtained (Le Roux and De Vleeschouwer 2010), before being digested following the above-mentioned protocol for AGV-2 and BHVO-2. Finally, for ATD, dissolution with a PAAR vessel was also performed to ensure, by comparison with the Savillex® procedure, that the dissolution was complete.

New multi-element separation scheme for dust isotopic signature

Our goal was to minimise the amount of material required for the chromatography and isotopic analyses by combining sequentially several columns. With a single aliquot, six elements – that is, Pb, Nd, Sr, Cu, Zn and Fe – were separated on seven successive columns, each of them with specific ion exchange resin (Figure 1). The chromatographic method was developed using adapted resins (mainly Bio-Rad AG1-X8 and AG50-X8), specifically designed for metal separation. Bio-Rad AG1-X8 and AG50-X8 are metal-free while being stable over time, resistant to light and easy to use (i.e., no re-suspension during loading). The Bio-Rad AG1-X8 resin is a strong anion exchange resin composed of polymerised styrene cross-linked by divinylbenzene (Kraus and Moore 1953). This resin is able to separate Cu, Fe and Zn thanks to their differences in speciation in concentrated HCl/HNO_3 solution, and elution schemes were first defined by Saito (1984) and Kraus and Nelson (1958) (see also Sossi *et al.* 2015 for a review) documenting the charts of ion exchange distribution coefficients with the considered acid and resin. The Bio-Rad AG50W-X8 resin is a strong cation exchange resin (composed of sulphonic acid functional groups), specifically designed for applications such as removal of cations and metals separations (Hoffer *et al.* 1979). The resins were pre-cleaned as follows: in a 250-ml closed PTFE vial (~ 6 cm diameter), a 2-cm thick layer of resin was first poured and a further layer (2–3 cm) of high-purity water was added on top before being gently shaken and let to rest for 1 h. Then,

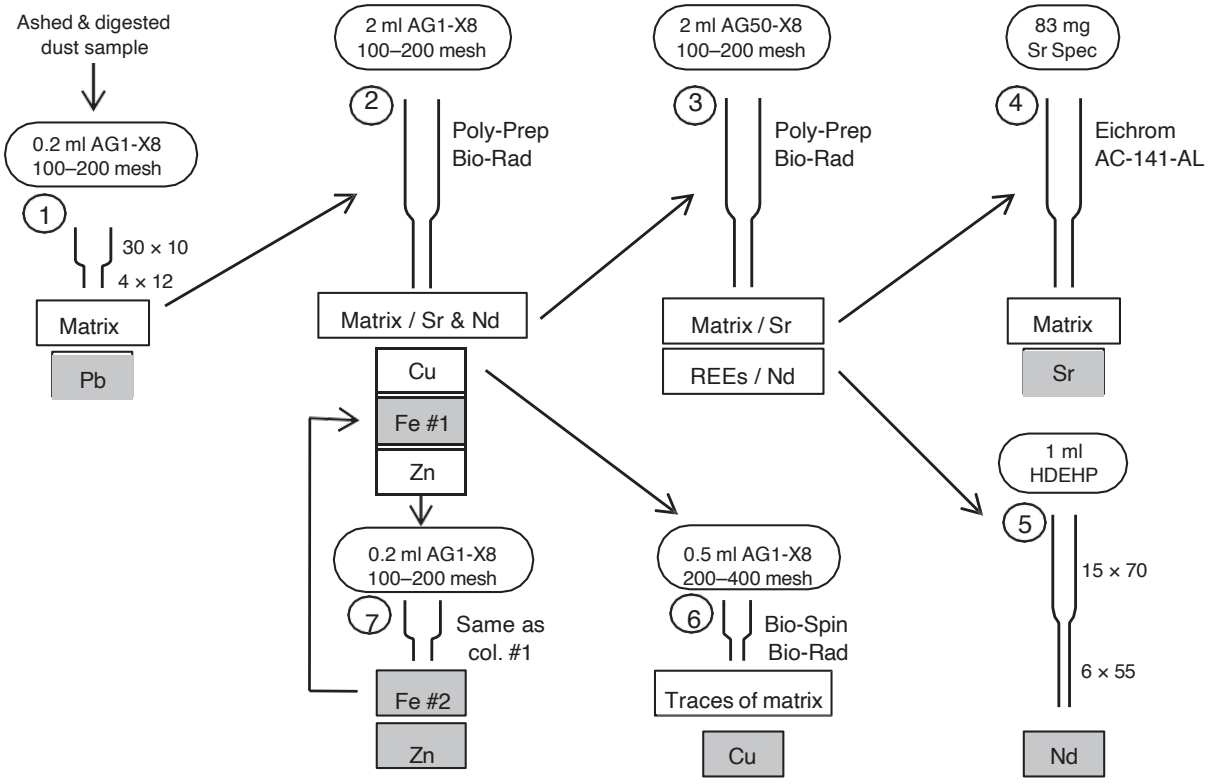

Figure 1. Chromatographic scheme to separate Pb, Nd, Sr, Zn, Cu and Fe. Circles represent step number (#). On the right of each column schematics, the column reference (for commercially available columns) or dimensions in mm ('inner diameter' 3 'height') of reservoir and resin bed for homemade columns is specified. The rounded-corner boxes indicate the resin used, while rectangular grey boxes symbolise the main elution steps for separated elements. 'Matrix' corresponds to all the other elements present in the solution at a given chromatographic step. Elution procedure and details are given in Table 2 and Table S1 and text.

Table 2.
Details of the elution scheme optimised for ATD following the sequence illustrated in Figure 1

Col #	Step	Acid	Elution volume [c] (ml)	Eluted elements => to be loaded on the next column	Blank (ng) [a]	Blank:sample ratio [b]	
						ATD	BCR-723
						(%)	
1	Loading + rinsing	0.5 mol l^{-1} HBr	1 + 9	Matrix => col. #2			
	Pb Elution	6 mol l^{-1} HCl	4	Pb	0.07	0.053	0.002
2	Loading + rinsing	0.6% H_2O_2 in 6 mol l^{-1} HCl + 6 mol l^{-1} HCl	1 + 3	Matrix => col. #3			
	Cu elution	8 mol l^{-1} HCl	56	Cu + traces of Ti, Mg, V => col. #6			
	Fe elution	0.5 mol l^{-1} HCl	20	Fe (99 %)			
	Zn elution	1 mol l^{-1} HNO_3/ 0.1 mol l^{-1} HBr	15	Zn + trace of Fe => col. #7			
3	Loading + rinsing	1.5 mol l^{-1} HCl	1 + 49	Matrix with Sr => col. #4			
	REE	6 mol l^{-1} HCl	20	REE => col. #5			
4	Loading + rinsing	2 + 2; 7 & 0.5 mol l^{-1} HNO_3	1 + 2; 3 & 1				
	Sr elution	0.05 mol l^{-1} HNO_3	2	Sr	0.40	0.036	0.047
5	Loading + rinsing	0.16 mol l^{-1} HCl	1 + 26				
	Nd elution	0.27 mol l^{-1} HCl	8	Nd	0.04	0.031	0.071
6	Loading + rinsing	0.6 % H_2O_2 in 8 mol l^{-1} HCl + 8 mol l^{-1} HCl	1 + 2	Ti, Mg, V			
	Cu elution	8 mol l^{-1} HCl	9	Cu	2.0	1.1	0.23
7	Loading + rinsing	6 mol l^{-1} HCl	1 + 1				
	Fe elution	1 mol l^{-1} HCl	4	Fe (last %) added to Fe from col. #2	19.7	0.016	0.016
	Zn elution	1 mol l^{-1} HNO_3/ 0.1 mol l^{-1} HBr	3	Zn	3.8	0.730	0.061

[a] 'Blank' corresponds to the mean total procedural blank values ($n = 4$).
[b] Blank:sample ratio for a 4 mg sample of ATD or BCR-723
[c] Details on elution procedure (comprising resin cleaning) available in Table S1.

the water supernatant was removed and a 2- to 3-cm layer of 6 mol l^{-1} HCl was added, gently shaken and again let to rest for 1 h. This cycle was repeated at least four times before one last cycle was performed with high-purity water. Ultimately, the pre-cleaned resin was stored with high-purity water at room temperature in a dark location. Resins were also cleaned and conditioned before sample loading as detailed in Table S1, where the whole chromatographic method is provided.

Before being loaded into a given column, the dried sample was systematically re-dissolved in the appropriate acid (as specified below) and then heated in a closed Savillex beaker for 5 min at 100 °C before being subjected to ultrasonication for 20 min. Before loading on col. #1 and col. #2, a centrifugation was applied (10000 RPM for 8 min – 560 *g*) to prevent clogging of the column. Elemental compositions and column recovery rates were determined using inductively coupled plasma-mass spectrometry (ICP-MS, Agilent 7700, Agilent Technologies, Santa Clara, CA, USA). Trace element measurements were calibrated using mix of mono-elemental standard solutions and USGS reference materials (BHVO-2 and AGV-2). Relative standard deviations (RSD) on replicates (same powder and dissolution, but repeated measurements) for Mg, Ti, V, Cr, Fe, Co, Ni, Cu, Rb, Sr, Cd, Ba, Pb and the rare earth element (REE) measurements were ≤ 5%, except Zn (< 7%).

Pb separation (col. #1): To prepare col. #1, 0.2 ml of fresh, pre-cleaned Bio-Rad AG1-X8 100–200 mesh resin (analytical grade, chloride form) was loaded into an in-house fabricated column (4 mm inner diameter by 1.2 cm height working bed and ~ 3 cm diameter by 1 cm height reservoir) (Figure 1). The resin was then rinsed several times with 2 ml of high-purity water, 0.5 mol l^{-1} HBr and 6 mol l^{-1} HCl (Table S1) before conditioning with 1 ml 0.5 mol l^{-1}

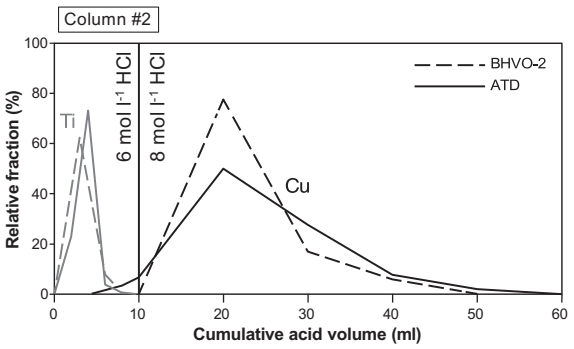

Figure 2. Representative Ti and Cu elution curves for BHVO-2 rock (dotted lines) and ATD dust (solid lines) reference materials. This comparison illustrates Ti (grey) and Cu (black) elution curves in column #2 using the BHVO-2 elution protocol. Using the latter protocol, ATD dust has typically a 'flattened' Cu elution peak compared with BHVO-2 highlighting the need for an optimised dust elution scheme.

HBr. Before loading, the dried digested samples were re-dissolved in 1 ml 0.5 mol l^{-1} HBr. At such HBr concentration, all elements from the matrix, except Pb, were eluted. Lead was recovered later by passing 6 mol l^{-1} HCl in col. #1 (Table 2) (e.g., Weis *et al.* 2006). The two eluates (i.e., matrix and Pb solutions) were dried down; Pb was stored for isotopic measurements, whereas the matrix solution was loaded onto col. #2.

Cu, Zn and Fe separation (cols #2, 6 and 7): The Bio-Rad AG1-X8 100–200 mesh resin (analytical grade, chloride form) was used to separate Cu, Fe and Zn, following a protocol modified from Mare'chal *et al.* (1999). The principle is based on differences in exchange distribution coefficients between elements on the resin. Typically, Zn and Fe (Fe^{3+}) will be retained on the resin and eluted later using low-molarity HCl or HNO_3. For Cu in high-molarity HCl – this was eluted at a slower rate than the matrix, allowing for its recovery. Briefly, in a standard Bio-Rad Poly-Prep® chromatography column, 2 ml of pre-cleaned AG1-X8 100–200 mesh resin (Figure 1) was successively rinsed in six cycles of 10 ml with high-purity water, 6 mol l^{-1} HCl and 1 mol l^{-1} HNO_3 (Table S1). The resin was then conditioned with 6 mol l^{-1} HCl, and to re-dissolve the matrix dry residue from the previous column, 1 ml 6 mol l^{-1} HCl with 20 µl of H_2O_2 was used. This solution was then loaded, and HCl (6 mol l^{-1}) was added to rinse out the matrix that contained Nd and Sr. Afterwards, 8 mol l^{-1} HCl was poured into the column to elute Cu. After a complete elution of Cu, 0.5 mol l^{-1} HCl was used to elute Fe. The potentially remaining Fe was recovered with Zn and ultimately separated via col. #7. Finally, Zn was eluted with 1 mol l^{-1} HNO_3/0.1 mol l^{-1} HBr (Table S1). Solutions that contain elements of interest were dried down before the next column or isotopic measurements (Table 2).

Particular attention was given to the separation of Cu as some major or trace elements (i.e., Ti, Mg, Fe, Na, Co, V and Ba), even at low level (e.g., Ti/Cu < 1), can affect the accuracy of isotope measurements (Petit *et al.* 2008, Liu *et al.* 2014). Because of incomplete Cu separation from the above-mentioned elements in col. #2 (Figure 2), we implemented a second step of separation (i.e., col. #6). Column #6 was prepared with 0.5 ml of fresh and pre-cleaned AG1-X8 200–400 mesh resin (analytical grade, chloride form) in a Bio-Rad (Bio-Spin® disposable) chromatography column. Then, successive rinsing cycles were performed with 4 ml of high-purity water, 6 mol l^{-1} HCl and 1 mol l^{-1} HNO_3, and was conditioned with 8 mol l^{-1} HCl. Copper dry residue from col. #2 was re-dissolved in 1 ml 8 mol l^{-1} HCl and 20 µl of H_2O_2 and loaded in col.# 6. Matrix and Cu were subsequently eluted in col. #6 with 8 mol l^{-1} HCl (Table 2). For Zn, we also performed an extra separation step (i.e., col. #7) to separate Zn from residual Fe (~ 1% of total Fe left in Zn elution fraction) and other potentially remaining elements (e.g., Mg, Ti and Ni; Chen *et al.* 2016). To prepare col. #7, 0.2 ml of fresh pre-cleaned Bio-Rad AG1-X8 resin (100–200 mesh, analytical grade, chloride form) loaded in a home-made column (same shape as col. #1) was cleaned and conditioned as for col. #2. Zinc dry residue from col. #2 was re-dissolved in 6 mol l^{-1} HCl and loaded into col. #7. Matrix was then eluted with 6 mol l^{-1} HCl. The residual Fe was eluted by 1 mol l^{-1} HCl and combined with the Fe elution fraction from col. #2. Finally, a 1 mol l^{-1} HNO_3/0.1 mol l^{-1} HBr mixture was used to elute Zn (Table 2).

Nd and Sr separation (cols #3, 4 and 5): To separate the REE from the matrix, 2 ml of fresh pre-cleaned Bio-Rad cation exchange AG50-X8 100–200 mesh (hydrogen form) resin was used in a Bio-Rad Poly-Prep® chromatography column (adapted from Weis *et al.* 2006) (Figure 1). This resin was rinsed in three cycles with 10 ml of high-purity water and 6 mol l^{-1} HCl before being conditioned with 10 ml 1.5 mol l^{-1} HCl (Table S1). The dried matrix from col. #2 containing Nd and Sr was re-dissolved in the same conditioning acid and loaded into column #3. The matrix (containing Sr) was eluted first in 1.5 mol l^{-1} HCl, while REE were eluted afterwards with 6 mol l^{-1} HCl (Table 2). These two cuts were dried down for further separation on cols. #4 and #5.

Separation of Nd from REE was performed in col. #5 (in-house constructed glass column 6 by 55-mm working bed and 15 ml reservoir) with in-house pre-calibrated HDEHP

resin (equivalent to the Eichrom Ln resin) according to the method of Richard *et al.* (1976). Neodymium was isolated from Ce and Sm because of isobaric interferences on ^{142}Nd and ^{144}Nd, respectively. Titrated 0.16 mol l^{-1} HCl was used for the conditioning of col. #5 and for re-dissolving the REE cut from col. #3. After sample loading, low atomic number REEs (La, Ce, Pr) were eluted with titrated 0.16 mol l^{-1} HCl, while Nd was eluted in titrated 0.27 mol l^{-1} HCl. Higher atomic number REEs were later eluted with 6 mol l^{-1} HCl.

Strontium was separated from the matrix on col. #4 (Figure 1) by the traditional method (described in Pin *et al.* 1994) using the Eichrom Sr resin (83 mg) in a 2 ml Eichrom column (AC-141-AL). Particular attention was given to separate Sr from Rb to avoid isobaric interferences. Col. #4 was made of 83 mg of fresh Sr resin, which was rinsed four times with 0.5 ml of 2 mol l^{-1} HNO_3. The same nitric acid was also used to re-dissolve dried-out matrix containing Sr, which was then loaded into col. #4 and later rinsed successively with 2, 7 and 3 mol l^{-1} HNO_3. Strontium was finally eluted in 0.05 mol l^{-1} HNO_3 (Table 2). Neodymium and Sr cuts were evaporated to dryness and kept for later isotopic measurements.

Isotopic determinations

Lead, Nd and Sr isotope ratios were measured using a Nu Plasma I (015), multi-collector-ICP-MS, while Zn, Cu, Fe were measured on a Nu Plasma II (233) High Resolution-MC-ICP-MS (Nu Instruments). The measurement sessions were spread over 2 years, from September 2015 to August 2017. Before isotopic measurement, each dried cut (preserved in Savillex vials) was re-dissolved in 20 Il of concentrated HNO_3, then evaporated and finally re-dissolved in 2 ml 0.05 mol l^{-1} HNO_3. The solution was heated at 100 °C for 20 min, then sonicated for 20 min and finally transferred into pre-cleaned microtubes and centrifuged. A typical measurement session started with a batch of repeated measurements (at least ten) of calibration solution to optimise the instrument. Concerning radiogenic isotopes, calibration solutions were measured after two samples and after each sample for heavy stable isotopes. At least three replicates were measured per sample (for Zn, Cu and Fe) and one replicate per sample for Pb, Nd and Sr.

Lead: A thallium dopant solution was added to every sample and NIST SRM 981 Pb calibrator solution to reach a ratio Pb:Tl of 6:1 (i.e., 125 ng ml^{-1} Pb and 25 ng ml^{-1} Tl). Close attention was paid to keep the Pb:Tl ratio constant for standards and samples to improve the reproducibility of the analytical conditions. All Pb analyses were conducted in wet plasma mode with a minimum ^{204}Pb signal intensity of 130 mV and a total beam of ~ 10 V (= 80 V per μg ml^{-1}). The use of the Aridus introduction system was not presently required to increase the sensitivity but can be applied for lower mass samples (as low as 5–10 ng). The ^{202}Hg beam intensity, consistently below 0.15 mV, was monitored to correct for these very low isobaric interferences of ^{204}Hg on ^{204}Pb. This correction was performed online applying equations detailed in Retzmann *et al.* (2017). Mass bias was corrected by external normalisation through Tl doping (Barling and Weis 2008) using a ^{205}Tl/^{203}Tl value of 2.3885 (Weis *et al.* 2006) and calibrator sample bracketing technique (CSB, or 'direct SSB' *sensu* Mason *et al.* 2004), applying the values of 36.7219 (^{208}Pb/^{204}Pb), 15.4963 (^{207}Pb/^{204}Pb) and 16.4905 (^{206}Pb/^{204}Pb) from Galer and Abouchami (1998). During the course of the study, repeated analyses of NIST SRM 981 provided mean values of 36.7246 ± 0.0161, 15.5016 ± 0.0032, 16.9343 ± 0.0048 (k = 2, see section 'Results of multi-isotopic analyses and estimation of measurement uncertainties'), n = 46), respectively, for ^{208}Pb/^{204}Pb, ^{207}Pb/^{204}Pb and ^{206}Pb/^{204}Pb. These results are in line with the long-term laboratory measurement repeatability of NBS-981 values and also data reported by Weis *et al.* (2006), respectively, of 36.7163 ± 0.0121, 15.4968 ± 0.0047 and 16.9407 ± 0.0036 (2s, n = 167). Long-term measurement repeatability of the laboratory for an in-house peat mix standard solution from 2018 to 2019 indicates good stability over time with values of 38.2756 ± 0.0091, 15.6249 ± 0.0030 and 18.2349 ± 0.0037 (k = 2, n = 24) for ^{208}Pb/^{204}Pb, ^{207}Pb/^{204}Pb and ^{206}Pb/^{204}Pb, respectively.

Neodymium: Our samples and the Rennes Nd calibrator solution (Chauvel and Blichert-Toft 2001) were diluted to a concentration of 200 ng ml^{-1} Nd reaching ~ 3 V on the ^{144}Nd mass. The analyses were performed in wet mode, but sample solutions as low as 10 ng ml^{-1} can also be measured using a dry plasma mode (Aridus, CETAC Technologies, Omaha, NE, USA). ^{147}Sm and ^{140}Ce were monitored to correct for isobaric interferences from ^{144}Sm, ^{148}Sm, ^{150}Sm and ^{142}Ce on Nd masses. Beam intensity of ^{147}Sm was below 0.1 mV implying a full separation of Sm from Nd. ^{140}Ce beam intensity was consistently below 0.05 V. These isobaric interference corrections were done online through established equations (e.g., Retzmann *et al.* 2017). Neodymium isotopic compositions were corrected by internal normalisation to the value of ^{146}Nd/^{144}Nd = 0.7219 (Hamilton *et al.* 1983); the CSB correction was applied relative to its internationally accepted value (^{143}Nd/^{144}Nd = 0.511961 ± 0.000013 (2s, n = 50), Chauvel and Blichert-Toft 2001). A mean value of ^{143}Nd/^{144}Nd = 0.511858 ± 0.000019 (k = 2, n = 31) was obtained for the Rennes Nd calibrator during our

sessions. Long-term measurement repeatability of the laboratory on a quality control JMC in-house standard solution from 2001 to 2018 indicates good stability over time with a $^{143}Nd/^{144}Nd$ value of 0.512227 ± 0.000021 (k = 2, n = 99).

Strontium: Sample solutions were diluted to achieve a Sr concentration of 120 ng ml^{-1} as in the Sr NBS 987 calibrator solution. The analyses were performed in wet mode with an intensity of 5.0 V measured on the ^{88}Sr mass. ^{83}Kr was monitored to correct for interference on ^{84}Sr and ^{86}Sr (Ehrlich *et al.* 2001); ^{83}Kr intensity was constantly below 0.05 mV. ^{85}Rb was also monitored to correct for isobaric interferences of ^{87}Rb on ^{87}Sr. The equations for this correction are available in Retzmann *et al.* (2017). The beam intensity of ^{85}Rb was systematically lower than 0.3 mV, thus confirming a negligible amount of Rb in the Sr solution (i.e., Rb:Sr ratio was maximum of ~ 0.006%). All the data were corrected for mass discrimination by internal normalisation using $^{86}Sr/^{88}Sr$ = 0.1194 and the CSB method. Repeated analyses of Sr NBS 987 yielded a mean value of $^{87}Sr/^{86}Sr$ = 0.710047 ± 0.000065 (k = 2, n = 25). CSB correction was applied using the $^{87}Sr/^{86}Sr$ value of 0.710252 ± 0.000013 (2s) from TIMS analyses (n = 88) (Weis *et al.* 2006). Long-term measurement repeatability of the laboratory on a Sr carbonate in-house standard solution from 2012 to 2019 indicates good stability over time with a $^{87}Sr/^{86}Sr$ value of 0.708388 ± 0.000047 (k = 2, n = 80).

Zinc and copper: The Cu/Zn-doping method (Marechal *et al.* 1999) was applied to the samples and the 'in-house' Cu and Zn calibration solutions. All the solutions were diluted to reach Zn and Cu concentrations of 400 ng ml^{-1}. Analyses were performed in wet plasma mode. Typically, the signal corresponded to ~ 2.3 V on the ^{64}Zn mass and ~ 5.0 V on the ^{63}Cu mass. ^{62}Ni ion beam intensity was monitored to correct for potential isobaric interferences of ^{64}Ni on ^{64}Zn and was consistently below 5 9 10^{-5} V, confirming the complete chemical separation of Ni from Zn and Cu solutions. The nickel interference was corrected online applying the approach and equations detailed in Rosman and Taylor (1998). Mass bias was corrected by applying the CSB method (*vs*. the in-house Cu and Zn calibrator), which was preferred yet still comparable to the ln($^{65}Cu/^{63}Cu$) *vs.* ln($^{66}Zn/^{64}Zn$) plot EEN correction method (Petit *et al.* 2008). The d/amu was also systematically calculated to monitor the mass-dependent discrimination between isotopes. The Zn and Cu isotopic compositions were reported in a delta (per mil) notation as shown by Equation (1):

$$\delta^{x}A_{\text{calibrator}} = \left(\frac{\delta^{x}A/^{y}A_{\text{sample}}}{\delta^{x}A/^{y}A_{\text{calibrator}}} - 1 \right) \quad (1)$$

where x corresponds to the higher mass and y is the lower mass for the same analyte (A) (e.g., $^{x}A = ^{66}Zn$ and $^{y}A = ^{64}Zn$ or $^{x}A = ^{65}Cu$ and $^{y}A = ^{63}Cu$). To compare with published Zn and Cu isotope data, our results were reported as $\delta^{66}Zn_{\text{JMC Lyon}}$ and $\delta^{65}Cu_{\text{NIST976}}$ relative to the Zn JMC-Lyon-03-0749l and Cu NIST SRM 976 calibrators, respectively, applying the equation of Hoefs (2004) as follows:

$$\delta_{\text{sample-}calA} = \left(\left\{ \frac{\delta_{calB\text{-}calA}}{1000} + 1 \right\} \left\{ \frac{\delta_{\text{sample-}calB}}{1000} + 1 \right\} - 1 \right) \quad (2)$$

where *calA* corresponds to the international calibrator Zn JMC-Lyon-03-0749l or Cu NIST SRM 976 and *calB* to the in-house calibrators, respectively. During analyses, repeated measurements of the in-house Zn and Cu calibrator solution gave a mean value of $\delta^{66}Zn$ = 0.00 ± 0.03‰ (k = 2, n = 121) and $\delta^{65}Cu$ = 0.00 ± 0.04‰ (k = 2, n = 107). The JMC-Lyon-03-0749l (doped with Cu NIST SRM 976) calibrator solution yielded $\delta^{66}Zn$ = +0.08 ± 0.03‰ (k = 2, n = 17) relative to the in-house Zn calibrator, while the calibrator Cu NIST SRM 976 (doped with Zn JMC-Lyon-03-0749l) gave a $\delta^{65}Cu$ of -1.24 ± 0.04‰ (k = 2, n = 4) compared with the in-house Cu calibrator. Finally, to evaluate the long-term external repeatability, the NIST SRM 976 solution provides a $\delta^{65}Cu_{\text{in-house}}$ of -1.06 ± 0.09‰ (k = 2, n = 129) from 2016 to 2019. The certified Zn IRMM-3702 solution (Ponzevera *et al.* 2006) was also measured to evaluate the long-term external repeatability throughout the Zn measurement sessions giving a mean $\delta^{66}Zn_{\text{JMC Lyon}}$ of +0.28 ± 0.05‰ (k = 2, n = 6). This result is in accordance with the laboratory long-term (2015–2017) value of +0.31 ± 0.07 (k = 2, n = 46) and in line with the literature ($\delta^{66}Zn_{\text{JMC Lyon}}$ = +0.28 ± 0.02‰ (weighted 2s); Archer *et al.* 2017). Further details about the Zn and Cu analytical method and corrections are given in Petit *et al.* (2008) and Mattielli *et al.* (2009).

Iron: Iron isotopic measurements were performed at medium resolution in dry mode using an Aridus II as desolvating sample inlet system. Iron samples were diluted to 800 ng ml^{-1} and doped with an in-house Ni solution. The CSB method using the IRMM-014 Fe calibrator solution was systematically applied for the mass bias correction. The d/amu was also systematically calculated. The notation of $\delta^{x}Fe$ is imitated from the Zn or Cu isotope expression (Equation 1) where $^{x}A = ^{56}Fe$ or ^{57}Fe and $^{y}A = ^{54}Fe$. A minimum intensity

of 14 V was obtained in the axial collector (^{56}Fe) for the IRMM-014. The ^{53}Cr beam intensity, which was monitored to circumvent potential spectral interferences, was consistently below 0.02 mV, implying complete removal of Cr during the separation scheme (i.e., Cr:Fe ratio corresponded to maximum 0.0001%). Chromium interference on mass 54 was corrected online following the method detailed in de Jong *et al.* (2007). During analytical sessions, the IRMM-014 measurements provided a mean value of $d^{56}Fe = 0.003 \pm 0.053‰$ ($k = 2$, $n = 89$). To evaluate the long-term repeatability of the laboratory, repeated measurements of an in-house carbonate mix standard provide $d^{56}Fe_{IRMM\text{-}014}$ value of -1.553 ± 0.98‰ ($k = 2$, $n = 129$) over 4 years (2014–2018). Further details of the Fe analytical methodology are given in de Jong *et al.* (2007).

Results and discussion: Validation scheme implemented

In this section, each step of the whole method is discussed in order to validate our implemented separation scheme, its versatility and adequacy with dust samples. This starts with the importance of removing the ubiquitous organic matter in dust without loss of material or contamination. Then, the dissolution step is checked to ensure the full dissolution of all minerals. Each chromatography step of the scheme is validated by the recovery rate (i.e., for ATD and BCR-723 matrix), hence providing a large versatility to our scheme for dust materials. Estimations of uncertainties via repetition of the entire procedure on multiple duplicates (different powder subsamples) are also provided, as well as an assessment of contamination degree through the elemental composition of total procedural blank and its potential effects on isotopic values. Finally, isotopic results are compared with values from previous studies, when available.

Sample ashing and dissolution

The removal of organic matter in dust sample is of critical importance for the quality of isotopic results. When present, organic matter can clog the column during the chromatographic separation and affect the chemistry by increasing the viscosity of the eluted fraction and by reducing the analyte recovery (leading to modification of the elution profile and retention time). Dust and typically anthropogenic dust contain organic matter (McTainsh and Strong 2007, Long *et al.* 2013) that can alter the accuracy of the elemental/isotopic composition measurements (e.g., Shiel *et al.* 2009). Two methods are usually applied in the literature: chemical oxidation (by addition of H_2O_2 or $HClO_4$) and 'ashing' ($T \sim 450$–500 °C). Chemical treatment – H_2O_2 – is costly and time-consuming as the amount of H_2O_2 needed differs from sample to sample, and might induce vigorous uncontrolled reactions and subsequent loss of sample solution. It also tends to increase the blank if used in large quantities. For instance, we measured a significant increase in metal in the blank when H_2O_2 was added (~ 0.5–1 ng of Zn, Cu or Pb per ml of Suprapur H_2O_2, which for Zn would represent up to 25% of total Zn from the procedural blank). Thus, we preferred to remove organic matter by thermal treatment in a muffle furnace, which offers two advantages: (a) the protocol is the same whatever the organic matter content is and (b) the total procedural blank value was minimised.

The efficiency of the acid dissolution is crucial and mainly depends on the mineralogy of the dust or rock sample. For instance, zircon and spinel phases, which are characterised by contrasting isotopic signature compared with the bulk sample, are difficult to dissolve (e.g., Weis *et al.* 2006, Rousseau *et al.* 2014). Whether or not these recalcitrant minerals fully dissolve during the acid digestion is essential to ensure reliable isotopic measurements, especially for reference materials such as G-2 where Pb isotopic ratios are controlled by the occurrence of zircons in this granite. Dust consists mainly of feldspar, quartz, clay minerals, carbonates, sulfates, phosphates, salts and also amphiboles and pyroxenes (e.g., Claquin *et al.* 1999, Formenti *et al.* 2014). However, the presence of zircon or other acid-resistant mineral grains cannot be excluded. For instance, Aarons *et al.* (2013) reported a 'zircon effect' in a Saharan dust storm event over the Atlantic. In order to check for the presence of acid-resistant minerals in ATD, we compared the dissolution efficiency using the Savillex beaker with the more aggressive PAAR high-pressure PTFE vessel digestion. All elements of interest (i.e., Pb, Nd, Sr, Zn, Cu and Fe) indicated identical elemental mass fractions, within the uncertainty range of ICP-MS analysis. Therefore, at least for ATD, Savillex® dissolution is appropriate. However, digestion in high-pressure PTFE vessels is recommended, especially where doubt exists regarding the dust sample mineralogy.

Chromatography: analyte separation and recovery

After the validation of the dissolution method, we tested the chromatographic scheme. Our strategy was (a) to validate an initial chromatographic method using three rock reference materials (BHVO-2, AGV-2 and G-2) for which elemental and isotopic data are available in the literature, (b) to apply this elution scheme on dust reference materials (ATD and BCR-723) with potential implementations and (c) to ultimately validate a dust-optimised chromatographic scheme through its application to natural dust samples

(Table 1). In order to evaluate our chromatographic scheme, we used extensively recovery rates that are mass fraction ratios of the element of interest measured in the elution fraction of interest normalised to the mass fraction of that element in the samples. The uncertainty associated with these ratios is a function of the uncertainty propagation and corresponds to 7, 6, 4, 9, 6 and 7%, respectively, for Pb, Nd, Sr, Zn, Cu and Fe.

BHVO-2, AGV-2 and G-2: Before any implementation of our initial chromatographic scheme, the analyte recovery for BHVO-2 was tested and systematically reached ~ 100% for the six elements of interest. In addition, no interfering element was detected in the elution fractions and no element of interest, analyte, was measured elsewhere than in the elution fraction of interest. The protocol was applied to AGV-2 and G-2, and the agreement of the obtained isotopic data with the literature (see section 'Results of multi-isotopic analyses and estimation of measurement uncertainties') confirmed that our methodology could be further tested on dust reference materials and samples.

ATD: Lead recovery was 103% in the elution fraction, and no Pb was detected in other elution fractions indicating that using rock protocol for ATD through col. #1 is appropriate, at least for Pb. As for Nd and Sr, recovery rates measured from their respective elution fractions reached, respectively, 92% and 81% and were free of interfering elements. Although rather low, the Sr and Nd recoveries for ATD do not affect the final accuracy and reproducibility of Sr and Nd isotopic ratios and are in fact preferred to larger elution volumes that might contain interfering elements (Richard *et al.* 1976). For non-traditional stable isotopes, Zn and Cu showed poor recovery rates of ~ 76% and ~ 87%, respectively. Iron recovery yielded 99% with the remaining 1% measured in the Zn elution fraction. As those non-traditional stable isotopes require full recovery to avoid biased isotopic ratio (Shiel *et al.* 2009, Petit *et al.* 2013) due to fractionation on the resin (Roe *et al.* 2003), we had to re-evaluate the chromatography schemes.

Several shifts in the elution peaks were identified, which are essentially due to changes in the matrix composition (distinct mineralogy and thus major element and organic contents). For instance, peak tailing was observed for Zn in col. #1 where Zn was partially (~ 10%) eluted in the Pb fraction. Concerning col. #2, 1% of total Fe was measured in the Zn elution fraction. In addition, as illustrated in Figure 2, the Cu elution peak of ATD in col. #2 is widened compared with the BHVO-2 Cu elution curve. Finally, Nd and Sr in ATD had their peaks shifted in cols. #4 and #5, which decreased their recovery rates. Following a re-calibration of the columns, Zn (col. #1) and Cu (col. #2) elution volumes were extended to recover their entire peaks. Also, 20 µl of H_2O_2 was added during the sample loading on cols. #2 and #6 (Figures 3a, b and Table 2) to minimise the matrix interfering elements (e.g., Ti in Figure 2) in the Cu cut (e.g., Blichert-Toft *et al.* 1997). A 60% decrease in Ti content was observed in Cu eluate when H_2O_2 was added. However, even with H_2O_2 addition, the Cu cut still contained significant amounts of Ti and Mg (Ti/Cu and Mg/Cu ~ 1) and some V (Figure 3a), which are known to produce spectral and non-spectral interferences significantly affecting accuracy of the Cu isotopic ratios (Petit *et al.* 2008, 2013, Liu *et al.* 2014). Consequently, an extra column (i.e., col. #6) was added to the chromatographic scheme to fully eliminate these matrix residues (Figure 3b and Table 2). To solve the Fe and Zn elution overlap issues (col. #2), we increased Fe elution duration and also raised the HCl molarity of the Fe elution from 0.5 to 1.5 mol l^{-1}, to elute Fe faster than Zn. The separation was significantly improved using 1 mol l^{-1} HCl to eluate Fe; however, even with increased Fe elution duration, Zn began to elute in the Fe fraction, meaning that the separation was still not optimal. Consequently, a second column (i.e., col. #7) was set up to definitively separate Zn from Fe and other potential matrix residue (Figure 3c). These modifications on col. #1, 2, 6 and 7 provided the full recovery of Zn, Cu and Fe, which were free of interfering elements and without any elements of interests spread across other elution fractions.

BCR-723: Subsequent to the re-calibration with ATD, the optimised scheme was tested on BCR-723, a road dust reference material, characterised by a very different chemical composition compared with ATD, with ~ 20 times more organic matter and mass fractions 25, 12 and 5 times higher in Pb, Zn and Cu, respectively (Table 1). With the ATD-optimised protocol, recovery rates for BCR-723 reached 99, 86, 83, 96, 101 and 100% for Pb, Nd, Sr, Zn, Cu and Fe, respectively. Based on our ATD chromatography where we identified several elution artefacts, we measured elemental composition of these potentially problematic elution fractions in the BCR-723 chromatography. The latter elution fractions of interest were all free of interfering elements, and no elements of interest were detected in any other elution fractions. In comparison, using the initial chromatographic scheme (i.e., optimised with BHVO-2), up to 35% of Zn, Cu and Fe were not recovered for BCR-723. This clearly demonstrates the need to adapt the initial chromatographic scheme (optimised with rock reference material, i.e., BHVO-2) to the dust reference materials (ATD and BCR-723).

Interestingly, we observed a large variability in elution time and peak profile in col. #2 depending on the different

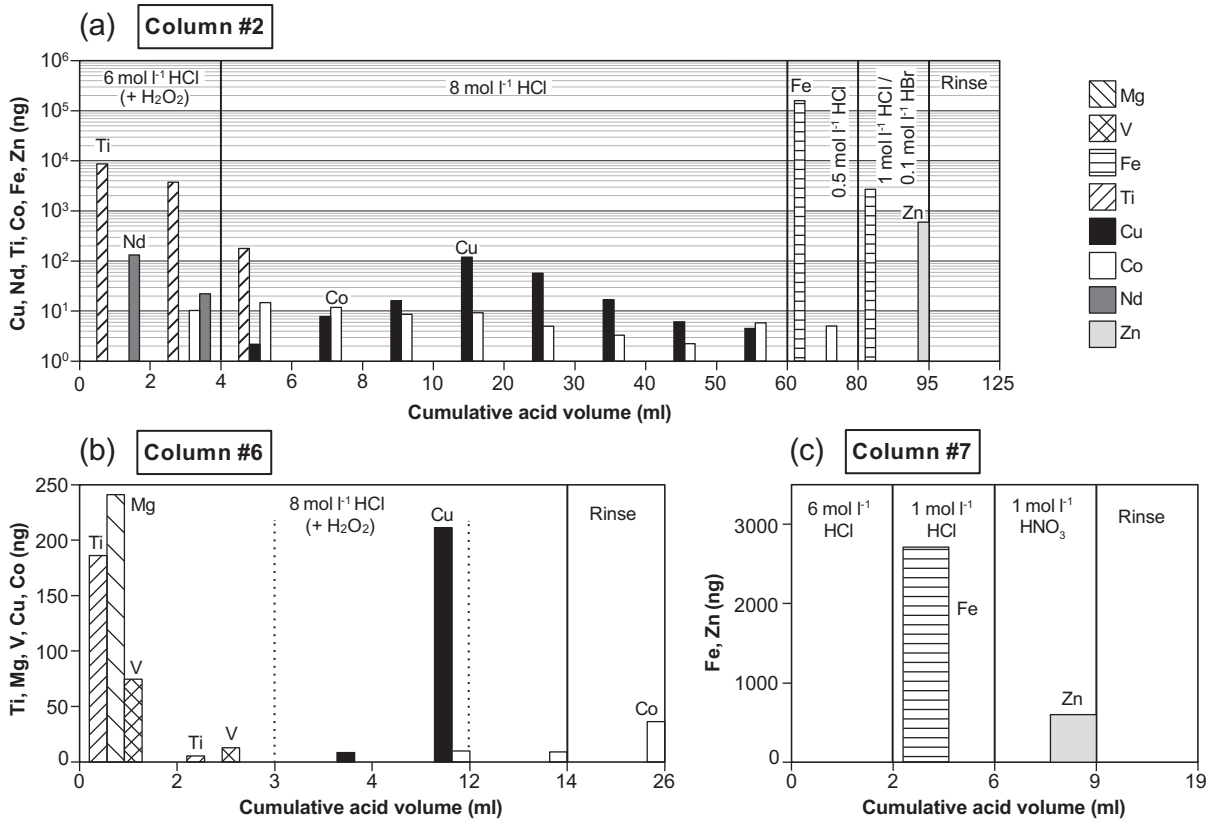

Figure 3. Optimised ATD elution scheme along columns #2, #6 and #7, respectively, shown in panels a–c. In (a), Mg and V are not shown but both have the same elution trend as Ti, and the same observation holds true for Sr with Nd. Solid vertical lines correspond to a change in eluent type or concentration, while dotted vertical lines represents changes in eluate composition. Note that the *x*-axis is not linear.

matrices (i.e., from BHVO-2, ATD and BCR-723), while in col. #6 and #7, all reference materials had exactly the same elution profile. Presumably, this observation is due to the removal of the matrix in a given sample. The last two columns for Cu and Zn separation (i.e., col. #6 and #7) guarantee the versatility to our chromatographic scheme, which is crucial for dust samples as their chemical composition, and thus matrices, can vary widely.

Natural dust samples: Considering the discrepancies between rock and dust reference materials in terms of chromatographic behaviour, separation recovery rates were tested on natural dust samples to optimise our chromatographic scheme to a wide range of dust samples. Samples from the Gobi, Sahara and Patagonia deserts (Table 1) were selected to represent the main source regions of mineral dust at the global scale. Results showed ~ 100% recoveries for Pb, 82–98% for Nd and 68–79% for Sr. These recovery rates, even for Sr, are high enough to ensure accurate and reproducible isotope analyses (Richard *et al.* 1976). Zinc (96–102%), Cu (95–96%) and Fe (94–105%) showed adequate recovery rates. However, after col. #2, a total of 2 to 4% of Fe was recovered in the Zn cut yielding a Fe/Zn ratio of 14, 10.5 and 9, respectively, for Patagonia, Sahara and Gobi dust samples. In their experiments, Chen *et al.* (2016) did not observe any modification of the zinc isotopic results for Fe/Zn ratios ≤ 10 but the effect of higher Fe/Zn is unknown. In our scheme, the presence of col. #7 ensured a complete separation of Fe from Zn and as such prevents any potential artefact of Fe on the accuracy of Zn isotopic measurement.

As a result, no interfering elements were measured in any final cut of any of the dust materials tested (i.e., ATD, BCR-723 and the three natural dust samples). Our chromatographic scheme is therefore adapted to dust materials that might display variable organic matter content and mineralogical composition (Table 1). For instance, the mass fraction of the Gobi sample was roughly five times higher than the Saharan natural dust precursor for the six elements

of interest. The largest mass fraction difference concerns Pb, where it is more than 250 times more abundant in BCR-723 relative to the Saharan natural dust sample.

In fact, our chromatographic scheme is not limited by the amount of dust sample. We successfully tested numerous amounts of dust from 4 to 25 mg, and they showed that the recovery rates did not vary across that mass range. The lower limit in terms of sample mass is controlled (a) by the mass fraction of the element of interest (i.e., lower mass fraction meaning higher dust mass needed) and (b) by the detection limit of the instrument (which will likely decrease in the near future). Therefore, in the case of unknown dust samples, we advocate for a pre-emptive total elemental determination (on sample aliquot) after digestion to evaluate the possibility of isotopic analysis depending on specific elemental mass available.

Procedural blanks: To evaluate the potential contamination during the entire chemical procedure (dissolution, multi-column elution scheme and evaporation steps) prior to the isotopic determination itself, repeated measurements of total procedural blanks ($n = 4$) were performed for the six analytes (Pb, Nd, Sr, Zn, Cu and Fe) (Table 2). Regarding Pb, the procedural blank was 0.07 ng which is substantially lower than the data published in Jweda *et al.* (2016) – 0.150 ng – and equivalent to Fourny *et al.* (2016) with 0.065 ng. For Nd and Sr, which were subjected to the largest number of elution cycles (i.e., 4), analyses of total procedural Sr and Nd blanks yielded mean values of 0.40 and 0.04 ng, respectively. Those values are significantly lower than the data (1.459 ng Sr and 0.145 ng Nd) recently reported in the literature (e.g., Fourny *et al.* 2016). For Zn, Cu and Fe, measurement of the mean total procedural blanks gave 3.8, 2.0 and 19.7 ng, respectively. Our three-column method for Cu separation gave comparable contamination values relative to those reported in Sossi *et al.* (2015) with a single column with AGI-X8 resin (1 ng) or Dong *et al.* (2013) who used two AG-MP1 resin columns for dust (2.4 ng). In contrast, the Zn amount from our procedural blank was about twice as large as the values reported in Sossi *et al.* (2015) and Dong *et al.* (2013), respectively, with 2 and 2.4 ng. A similar pattern was also observed for Fe, with 10 ng in Sossi *et al.* (2015) compared with 19.7 ng Fe in our study. Overall, the contamination degree related to our procedure seems to be holding at the level of those obtained in recent publications (mostly using single-column schemes) despite the use of a multi-column scheme in our case.

In terms of contamination, the most critical steps are related to the opening of the vials (during the multiple evaporation steps), which should be minimised. This is especially true for Zn, which can be easily contaminated even in clean laboratory conditions. Thus, in order to estimate the potential contamination contribution on the samples, trace element abundance ratios between blank and sample (blank:sample) were calculated for a 4 mg sample of ATD or BCR-723 (Table 2). All blank:sample ratios were ≤ 1%, and most of them were < 0.1% hence confirming that our chemical procedure did not affect the isotopic measurements.

Considering our high recovery rates and the low-level of our procedural contamination, we advocate a multi-column scheme instead of a single-column method (e.g., Pin *et al.* 2014, Sossi *et al.* 2015, Retzmann *et al.* 2017). The choice of adding columns, which increases handling, is here supported by the low procedural blank value and the versatility of the method adapted to a wide diversity of dust samples. As such, our multi-column scheme appears more reliable to ensure accurate, precise and reproducible isotope measurement results for compositionally variable dust compared with a single column where elution profiles can easily shift and overlap, hence compromising analyte separation.

Results of multi-isotopic analyses and estimation of measurement uncertainties

The combined uncertainties on isotope ratios were estimated as equivalent to the standard deviation of multiple measurements of duplicates (that varied from 2 to 6, see 'nd' values in Tables 3–8). Duplicates consist here of distinct sub sample powders from a given reference material, which underwent the exact same analytical procedure from initial weighing to final isotopic determinations (including separated ashing, digestion and multi-column chromatography). The expanded uncertainties with a coverage factor of 2, noted U ($k = 2$), were calculated as follows:

$$U(k = 2) = 2 \times \sqrt{\frac{\sum (x - \bar{x})^2}{(n-1)}} \quad (3)$$

where x is a given isotopic measurement, $\bar{x}$ is the mean and n is the total number of measurements.

The combined uncertainty estimated on measurements of duplicates combines the main contributions of uncertainties associated with instrumental effects (e.g., drift, variability within a single measurement session and also between sessions) and also random errors in the whole procedure (e.g., potential contamination, handling error).

Table 3.
Lead isotopic composition of rock and dust reference materials

Samples # [a]	$^{208}Pb/^{204}Pb$	U (k = 2) [d]	$^{207}Pb/^{204}Pb$	U (k = 2) [d]	$^{206}Pb/^{204}Pb$	U (k = 2) [d]
AGV-2						
AGV-2_1_rep1	38.5426	0.0023	15.6166	0.0008	18.8691	0.0009
AGV-2_1_rep2	38.5444	0.0020	15.6178	0.0007	18.8708	0.0007
AGV-2_1_rep3	38.5455	0.0027	15.6169	0.0010	18.8695	0.0009
Mean AGV-2_1	38.5441	0.0029	15.6171	0.0013	18.8698	0.0018
AGV-2_2_rep1	38.5448	0.0022	15.6161	0.0009	18.8718	0.0009
AGV-2_2_rep2	38.5413	0.0033	15.6157	0.0012	18.8716	0.0016
Mean AGV-2_2	38.5431	0.0049	15.6159	0.0006	18.8717	0.0003
Mean of the duplicates (nd = 2) [b]	*38.5436*	*0.0015*	*15.6165*	*0.0017*	*18.8708*	*0.0027*
G-2						
G-2_1_rep1	38.8928	0.0028	15.6361	0.0008	18.3987	0.0010
G-2_1_rep2	38.8927	0.0023	15.6350	0.0008	18.3980	0.0009
G-2_1_rep3	38.8958	0.0029	15.6351	0.0011	18.3981	0.0010
Mean G-2_1 (S) [c]	38.8938	0.0036	15.6354	0.0012	18.3983	0.0008
G-2_2 (P) [c]	38.8980	0.0025	15.6349	0.0008	18.3902	0.0008
G-2_3 (P) [c]	38.8931	0.0024	15.6322	0.0009	18.4053	0.0010
Mean of the (P) duplicates (nd = 2) [b]	*38.8955*	*0.0070*	*15.6335*	*0.0038*	*18.3978*	*0.0213*
ATD						
ATD_1	38.5822	0.0018	15.6264	0.0007	18.8292	0.0009
ATD_2	38.5837	0.0021	15.6271	0.0008	18.8280	0.0009
ATD_3	38.5856	0.0019	15.6278	0.0007	18.8308	0.0008
ATD_4	38.5915	0.0026	15.6296	0.0009	18.8316	0.0011
Mean of the duplicates (nd = 4) [b]	*38.5858*	*0.0082*	*15.6277*	*0.0027*	*18.8299*	*0.0033*
BCR-723						
BCR-723_1_rep1	37.2215	0.0028	15.5551	0.0010	17.4002	0.0009
BCR-723_1_rep2	37.2208	0.0023	15.5557	0.0008	17.4014	0.0007
Mean BCR-723_1	37.2211	0.0009	15.5554	0.0008	17.4008	0.0017
BCR-723_2_rep1	37.2230	0.0027	15.5560	0.0009	17.4011	0.0008
BCR-723_2_rep2	37.2224	0.0029	15.5556	0.0011	17.3997	0.0011
Mean BCR-723_2	37.2227	0.0009	15.5558	0.0006	17.4004	0.0020
BCR-723_3_rep1	37.2256	0.0022	15.5551	0.0010	17.4017	0.0008
BCR-723_3_rep2	37.2256	0.0027	15.5551	0.0010	17.4022	0.0015
Mean BCR-723_3	37.2256	0.0001	15.5551	0.0001	17.4020	0.0007
BCR-723_4_rep1	37.2231	0.0028	15.5557	0.0011	17.4015	0.0011
BCR-723_4_rep2	37.2272	0.0018	15.5571	0.0006	17.4019	0.0007
Mean BCR-723_4	37.2252	0.0058	15.5564	0.0019	17.4017	0.0006
BCR-723_5_rep1	37.2215	0.0026	15.5555	0.0009	17.4002	0.0008
BCR-723_5_rep2	37.2243	0.0024	15.5554	0.0009	17.3996	0.0009
Mean BCR-723_5	37.2229	0.0040	15.5555	0.0002	17.3999	0.0009
BCR-723_6	37.2238	0.0026	15.5549	0.0008	17.3992	0.0006
Mean of the duplicates (nd = 6) [b]	*37.2235*	*0.0033*	*15.5555*	*0.0011*	*17.4007*	*0.0021*

Regular font corresponds to a single analysis (three cycles of twenty runs for radiogenic isotopes or a triplicate for Zn, Cu and Fe isotopic results), bold font corresponds to the value of one duplicate (from a single replicate or several replicates), and bold and italic font corresponds to the mean of several duplicates.

[a] 'name_duplicate#_replicate#' corresponds to the results (regular font) obtained from each replicates (same powder, dissolution and chemical procedure, but repeated measurements).

[b] 'nd' corresponds to the number of duplicates (total procedure performed on different powder subsamples) used to calculate the overall mean reported for a given sample.

[c] (S) indicates dissolution in Savillex and (P) for dissolution in PAAR high-pressure PTFE vessel.

[d] U (k = 2) calculated via Equation (3) is the expanded uncertainty (k = 2) at 95% confidence level.

Having said that, this combined uncertainty does not take into account several other potential systematic sources of uncertainty such as (a) powder contamination of ATD and BCR-723 materials, (b) contamination of calibrator and dopant solutions (however, this was not detected through our in-house long-term measurement repeatability), (c) effects of

Table 4.
Neodymium isotopic composition of rock and dust reference materials

Samples # [a]	$^{143}Nd/^{144}Nd$	U (k = 2) [d]
AGV-2		
AGV-2_1	0.512785	0.000006
AGV-2_2_rep1	0.512774	0.000009
AGV-2_2_rep2	0.512777	0.000011
Mean AGV-2_2	0.512776	0.000005
AGV-2_3	0.512785	0.000007
Mean of the duplicates (nd = 3) [b]	*0.512782*	*0.000011*
G-2		
G-2_1_rep1	0.512228	0.000005
G-2_1_rep2	0.512227	0.000007
Mean G-2_1 (S) [c]	0.512227	0.000001
G-2_2 (P) [c]	0.512247	0.000013
G-2_3_rep1	0.512216	0.000006
G-2_3_rep2	0.512219	0.000005
G-2_3_rep3	0.512231	0.000005
Mean G-2_3 (P) [c]	0.512222	0.000016
Mean of the duplicates (nd = 4) [b]	*0.512232*	*0.000027*
ATD		
ATD_1_rep1	0.512144	0.000005
ATD_1_rep2	0.512145	0.000006
ATD_1_rep3	0.512143	0.000006
ATD_1_rep4	0.512158	0.000005
Mean ATD_1	0.512148	0.000014
ATD_2_rep1	0.512159	0.000006
ATD_2_rep2	0.512167	0.000004
ATD_2_rep3	0.512150	0.000004
ATD_2_rep4	0.512149	0.000005
Mean ATD_2	0.512156	0.000017
ATD_3_rep1	0.512154	0.000004
ATD_3_rep2	0.512150	0.000004
ATD_3_rep3	0.512154	0.000003
ATD_3_rep4	0.512145	0.000011
Mean ATD_3	0.512151	0.000009
ATD_4_rep1	0.512154	0.000004
ATD_4_rep2	0.512159	0.000003
ATD_4_rep3	0.512151	0.000003
ATD_4_rep4	0.512151	0.000004
Mean ATD_4	0.512154	0.000008
Mean of the duplicates (nd = 4) [b]	*0.512152*	*0.000008*
BCR-723		
BCR-723_1_rep1	0.512231	0.000004
BCR-723_1_rep2	0.512232	0.000007
Mean BCR-723_1	0.512231	0.000002
BCR-723_2_rep1	0.512231	0.000007
BCR-723_2_rep2	0.512223	0.000005
Mean BCR-723_2	0.512227	0.000011
BCR-723_3	0.512212	0.000004
BCR-723_4	0.512219	0.000010
BCR-723_5	0.512214	0.000005
BCR-723_6	0.512216	0.000010
Mean of the duplicates (nd = 6) [b]	*0.512220*	*0.000016*

For footnotes, see Table 3.

Table 5.
Strontium isotopic composition of rock and dust reference materials

Samples # [a]	$^{87}Sr/^{86}Sr$	U (k = 2) [d]
AGV-2		
AGV-2_1	0.703982	0.000020
AGV-2_2	0.703994	0.000013
AGV-2_3	0.703990	0.000016
Mean of the duplicates (nd = 3) [b]	*0.703989*	*0.000012*
G-2		
G-2_1 (S) [c]	0.709765	0.000020
G-2_2 (P) [c]	0.709765	0.000017
G-2 _3_rep1	0.709762	0.000015
G-2_3_rep2	0.709759	0.000009
G-2_3_rep3	0.709757	0.000010
Mean G-2_3 (P) [c]	0.709759	0.000006
Mean of the duplicates (nd = 3) [b]	*0.709763*	*0.000007*
ATD		
ATD_2_rep1	0.715777	0.000010
ATD_2_rep1	0.715780	0.000012
ATD_2_rep1	0.715764	0.000012
Mean ATD_2	0.715774	0.000017
ATD_3_rep1	0.715785	0.000013
ATD_3_rep2	0.715782	0.000011
Mean ATD_3	0.715783	0.000004
ATD_4_rep1	0.715791	0.000003
ATD_4_rep2	0.715793	0.000003
ATD_4_rep3	0.715798	0.000003
Mean ATD_4	0.715794	0.000007
Mean of the duplicates (nd = 3) [b]	*0.715784*	*0.000020*
BCR-723		
BCR-723_1	0.710110	0.000017
BCR-723_2	0.710102	0.000019
BCR-723_4	0.710101	0.000019
BCR-723_5	0.710096	0.000015
BCR-723_6	0.710109	0.000015
Mean of the duplicates (nd = 5) [b]	*0.710104*	*0.000012*

For footnotes, see Table 3.

environmental conditions on the instrument such as room temperature, humidity, plasma temperature, (d) estimation of constants and parameters for correction laws, IUPAC masses, calibrator and dopant (we typically used general consensus values from literature, see section 'Isotopic determinations'), and (e) systematic contamination effects. The impact of the latter can be estimated via a mixing calculation as follows (John and Adkins 2010):

$$a_{sample} = a_{dust} \times (1 - f_{contaminant}) + a_{blank} \times f_{contaminant} \quad (4)$$

where *a* corresponds to the isotopic value (i.e., Pb, Nd, Sr isotopic ratio or $\delta^{66}Zn$, $\delta^{65}Cu$, $\delta^{56}Fe$ value) of the contaminated sample (a_{sample}), the pristine dust sample (a_{dust}) or the

Table 6.
Zinc isotopic composition of rock and dust reference materials

Samples # [a]	$d^{66}Zn_{JMC\ Lyon}$ (‰)	U (k = 2) [d]	n	damu
AGV-2				
AGV-2_1_rep1	0.31	0.03	2	1.2
AGV-2_1_rep2	0.28	0.02	3	1.0
Mean AGV-2_1	0.30	0.04		
AGV-2_2	0.24	0.08	3	0.8
Mean of the duplicates (nd = 2) [b]	*0.27*	*0.08*	*8*	
G-2				
G-2_1 (S) [c]	0.34	0.03	3	1.0
G-2_2 (P) [c]	0.29	0.04	2	0.9
G-2_3 (P) [c]	0.29	0.05	3	0.9
G-2_4 (P) [c]	0.29	0.04	3	1.0
Mean of the duplicates (nd = 4) [b]	*0.30*	*0.05*	*11*	
ATD				
ATD_1	0.18	0.04	3	1.0
ATD_2	0.16	0.03	3	1.0
ATD_3	0.20	0.02	3	1.0
Mean of the duplicates (nd = 3) [b]	*0.18*	*0.04*	*9*	
BCR-723				
BCR-723_1	0.13	0.03	3	1.1
BCR-723_2	0.17	0.03	3	1.1
BCR-723_3_rep1	0.10	0.05	3	0.9
BCR-723_3_rep2	0.10	0.03	3	0.8
Mean BCR-723_3	0.10	0.05		
BCR-723_5_rep1	0.10	0.02	4	0.8
BCR-723_5_rep2	0.09	0.02	3	1.1
Mean BCR-723_5	0.10	0.01		
BCR-723_6_rep1	0.11	0.02	3	0.9
BCR-723_6_rep2	0.10	0.02	3	1.0
Mean BCR-723_6	0.11	0.01		
Mean of the duplicates (nd = 5) [b]	*0.13*	*0.06*	*25*	

For footnotes, see Table 3.

Table 7.
Copper isotopic composition of rock and dust reference materials

Samples # [a]	$d^{65}Cu_{NIST\ 976}$ (‰)	U (k = 2) [d]	n
AGV-2			
AGV-2_1	0.13	0.03	4
AGV-2-2	-0.05	0.02	3
Mean of the duplicates (nd = 2) [b]	*0.04*	*0.26*	*7*
G-2			
G-2 (S) [c]	0.29	0.04	3
ATD			
ATD_1	0.37	0.02	3
ATD_2	0.30	0.04	4
ATD_3	0.36	0.04	4
Mean of the duplicates (nd = 3) [b]	*0.34*	*0.07*	*11*
BCR-723			
BCR-723_5_rep1	-0.18	0.02	3
BCR-723_5_rep2	-0.14	0.01	3
Mean BCR-723_5	-0.16	0.05	
BCR-723_6_rep1	-0.16	0.04	3
BCR-723_6_rep2	-0.15	0.03	3
Mean BCR-723_6	-0.15	0.01	
Mean of the duplicates (nd = 2) [b]	*-0.16*	*0.01*	*12*

For footnotes, see Table 3.

contaminant (a_{blank}). $f_{contaminant}$ corresponds to the normalised mass fraction of contaminant in the contaminated sample, defined as follows:

$$f_{contaminant} = \frac{m_{i(blank)}}{m_{i(dust)} + m_{i(blank)}} \quad (5)$$

where m_i is the elemental mass in the pristine dust sample and in the blank (in ng, Table 2). According to Equations (4) and (5), any increase in the blank:dust ratio or in the isotopic offset between a_{dust} and a_{blank} will cause a more pronounced contamination (i.e., difference between pristine dust (a_{dust}) and contaminated sample (a_{sample})). Regarding contamination effects, Pb is certainly the most sensitive among the radiogenic isotopic systems, as is Zn for non-traditional stable isotopes. In what follows we estimated the impact of contamination effects for Pb and Zn using, respectively, (a) a $^{207}Pb/^{204}Pb$ value of 15.695 measured in a blank in our laboratory, and (b) a $d^{66}Zn_{JMC\ Lyon}$ value of 0.13‰ observed in coins and enriched ores, the most representative potential sources of Zn contamination (John *et al.* 2007, Mattielli *et al.* 2009). For 4 mg of ATD, the difference between a_{sample} and a_{dust} would amount to 0.00004 for $^{207}Pb/^{204}Pb$ and 0.0004‰ for $d^{66}Zn$, thus indicating a negligible contamination effect on those isotopic measurements. Overall in ATD and BCR-723, even though the sample mass considered is low (4 mg), our calculations show that contamination does not significantly influence the dust isotopic signature and can thus be neglected in the combined uncertainty assessment.

To reach a substantial contamination level – for instance a 0.01‰ difference in $d^{66}Zn$ (~ 25% of the combined uncertainty estimated for ATD) – three terms should be considered according to Equations (4 and 5): elemental mass in blank ($m_{i(blank)}$), its isotopic signature a_{blank} and the elemental mass in dust ($m_{i(dust)}$). For a given value of $m_{i(dust)}$ (i.e., 4 mg) and a a_{blank} of 0.13‰, $m_{i(blank)}$ would need to reach a mass equivalent to 130 ng (currently, 3.8 ng). Alternatively, this 0.01‰ difference in $d^{66}Zn$ could be achieved by shifting the a_{blank} value from the current 0.13‰ to ~ 1.5‰. Similarly, in the case of ATD,

Table 8.
Iron isotopic composition of rock and dust reference materials

Samples # [a]	$d^{56}Fe_{IRMM014}$	U (k = 2) [d]	$d^{57}Fe_{IRMM014}$	U (k = 2) [d]	n
AGV-2					
AGV-2_1	0.127	0.045	0.138	0.117	4
AGV-2_2	0.116	0.063	0.152	0.064	4
AGV-2_3	0.117	0.061	0.142	0.140	3
Mean of the duplicates (nd = 3) [b]	*0.120*	*0.012*	*0.144*	*0.015*	*11*
G-2					
G-2_1 (S) [c]	0.150	0.023	0.256	0.042	2
G-2_2 (P) [c]	0.164	0.057	0.267	0.081	3
G-2_3 (P) [c]	0.185	0.008	0.206	0.057	2
Mean of the duplicates (nd = 3) [b]	*0.166*	*0.036*	*0.243*	*0.064*	*7*
ATD					
ATD_1	-0.051	0.035	-0.090	0.062	3
ATD_2	-0.069	0.011	-0.106	0.023	3
ATD_3	-0.081	0.026	-0.120	0.041	3
ATD_4	-0.024	0.041	-0.113	0.244	3
Mean of the duplicates (nd = 4) [b]	*-0.057*	*0.049*	*-0.107*	*0.026*	*12*
BCR-723					
BCR-723_2	0.037	0.046	0.045	0.077	3
BCR-723_3_rep1	0.103	0.091	0.163	0.137	2
BCR-723_3_rep2	0.072	0.079	0.116	0.084	3
Mean BCR-723_3	0.087	0.022	0.140	0.033	
BCR-723_4	0.054	0.077	0.068	0.105	3
BCR-723_5	0.066	0.078	0.061	0.072	3
BCR-723_6_rep1	0.064	0.006	0.121	0.138	2
BCR-723_6_rep2	0.086	0.067	0.079	0.051	3
Mean BCR-723_6	0.075	0.016	0.100	0.029	
Mean of the duplicates (nd = 5) [b]	*0.064*	*0.039*	*0.083*	*0.075*	*19*

For footnotes, see Table 3.

$m_{i(dust)}$ could be as low as 0.12 mg before that contamination leads to a difference of 0.01‰ in $d^{66}Zn$. Mainly due to higher metal mass fraction in BCR-723, the contamination level was at least two times lower relative to ATD. Overall for ATD and BCR-723, considering that the $m_{i(blank)}$ and its associated isotopic composition (a_{blank}) are unlikely to vary significantly, these calculations clearly show that our scheme could be applied to much lower masses of dust sample (i.e., $m_{i(dust)}$).

AGV-2 and G-2: Accuracy of the measurements was evaluated by comparing our data from rock reference materials with those from the literature. For AGV-2, our mean value in $^{206}Pb/^{204}Pb$ (18.8708 ± 0.0027 (k = 2)), $^{207}Pb/^{204}Pb$ (15.6165 ± 0.0017) and $^{208}Pb/^{204}Pb$ (38.5436 ± 0.0015) (Table 3) obtained from three duplicates was in agreement with the 18.8688 ± 0.0063, 15.6173 ± 0.0071 and 38.5443 ± 0.0135 (2s), respectively, reported by Weis *et al.* (2006). A similar match was observed for $^{143}Nd/^{144}Nd$ and $^{87}Sr/^{86}Sr$ data (0.512782 ± 0.000011 and 0.703989 ± 0.000012 (k = 2), respectively; Tables 4 and 5) compared to Weis *et al.* (2006) reporting, respectively, 0.512790 ± 0.000016 and 0.703981 ± 0.000016 (2s).

The Pb isotopic data from G-2 can be divided into two categories depending on the digestion method used: Savillex (S) and high-pressure PAAR vessel (P) (Table 3). Weis *et al.* (2006) reported a discrepancy between these two digestion methods for G-2, where the typical digestion using Savillex yields more radiogenic values ($^{207}Pb/^{204}Pb$ of 15.6361 ± 0.0049 (2s) (S)) than for PAAR dissolution ($^{207}Pb/^{204}Pb$ = 15.6353 ± 0.0025 (2s) (P)). This is likely due to the presence of resistant minerals in the G-2 granitic rock. Similarly, our results exhibit slightly different $^{207}Pb/^{204}Pb$ values with 15.6354 ± 0.0012 (k = 2) (S), more radiogenic than 15.6335 ± 0.0038 (k = 2) (P). The same trend can be observed for $^{206}Pb/^{204}Pb$ and $^{208}Pb/^{204}Pb$ ratios (Table 3), however, to a much lesser extent (within the

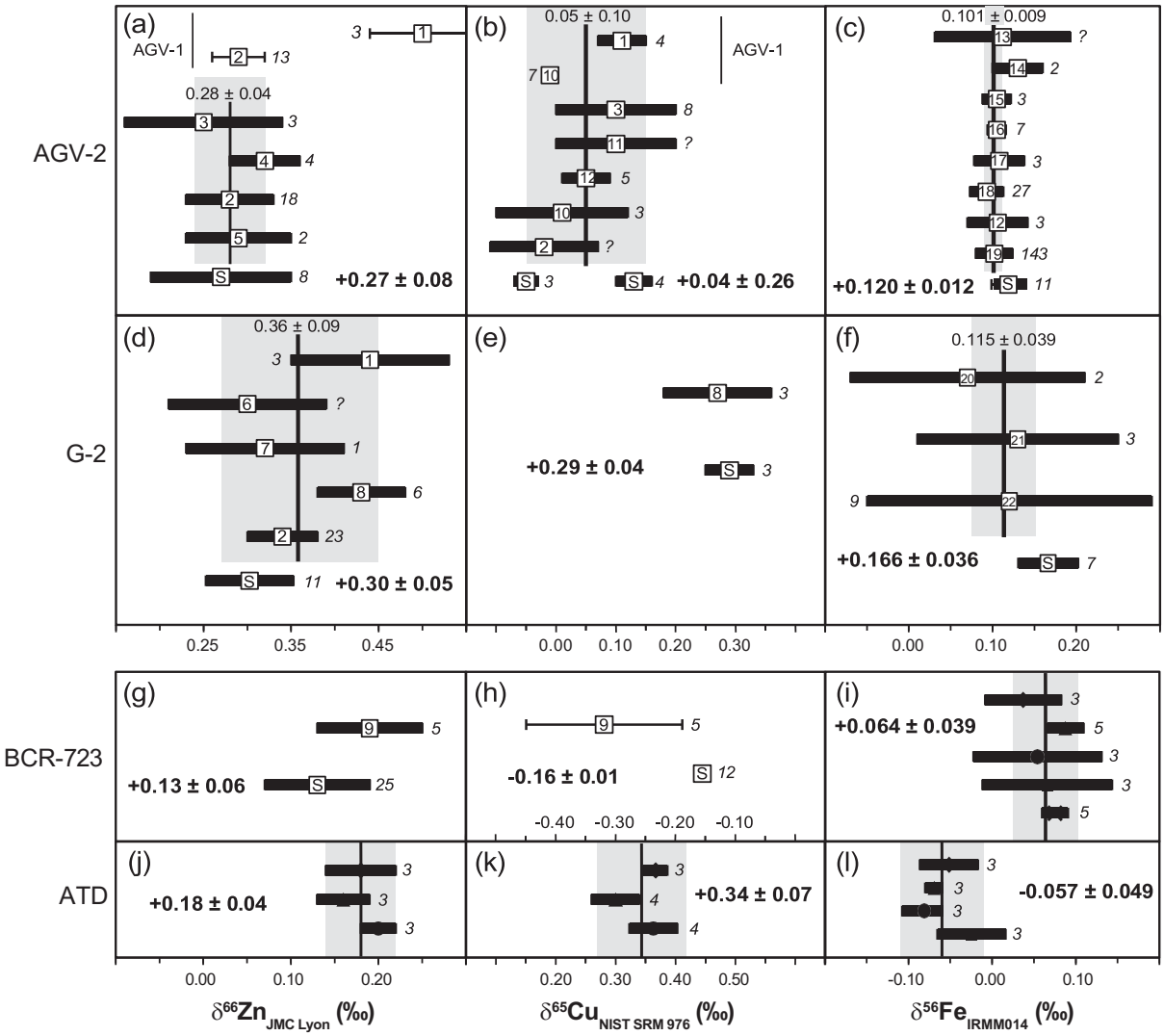

Figure 4. Compilation of $d^{66}Zn_{JMC\ Lyon}$, $d^{65}Cu_{NIST976}$ and $d^{56}Fe_{IRMM014}$ data for AGV-2 and G-2 rock reference materials as well as for the dust reference materials ATD and BCR-723. The black vertical line and the shaded area correspond to the weighted mean (by number of replicates) and the associated 2*s* of the literature data. Numbers in squares refer to literature references listed below (precision statements specified in the reported literature are expressed as 2*s* or 2r). 'S' in squares represents the mean values of the duplicates and *U* (*k* = 2) in our study (values in bold). Solid symbols correspond to the different duplicates from this study when there are no data available in the literature. Italic numbers associated with uncertainty bars are the number of replicates analysed in the corresponding study. (1) Moeller *et al.* (2012); (2) Chen *et al.* (2016); (3) Moynier *et al.* (2010); (4) Chen *et al.* (2013); (5) Arau'jo *et al.* (2017); (6) Paniello *et al.* (2012b); (7) Paniello *et al.* (2012a); (8) Dong *et al.* (2013); (9) Dong *et al.* (2017); (10) Savage *et al.* (2015) (mean of the duplicates for AGV-1); (11) Weinstein *et al.* (2011); (12) Liu *et al.* (2014); (13) Dauphas *et al.* (2004); (14) Dideriksen *et al.* (2006) (mean of the duplicates); (15) Dauphas *et al.* (2009); (16) Craddock and Dauphas (2011); (17) Millet *et al.* (2012); (18) Wang *et al.* (2012); (19) He *et al.* (2015); (20) Beard *et al.* (2003); (21) Chapman *et al.* (2009); (22) Fehr *et al.* (2008).

expanded uncertainty (*k* = 2)). Neodymium or Sr isotopic results for G-2 showed no significant difference between Savillex or PAAR dissolution. The measured values of $^{143}Nd/^{144}Nd = 0.512232 \pm 0.000027$ (*k* = 2) and $^{87}Sr/^{86}Sr = 0.709763 \pm 0.000007$ (*k* = 2) (Tables 4 and 5) are in line with the data reported by Weis *et al.* (2006) with 0.512222 ± 0.000006 (2*s*) and 0.709770 ± 0.000014 (2*s*), respectively.

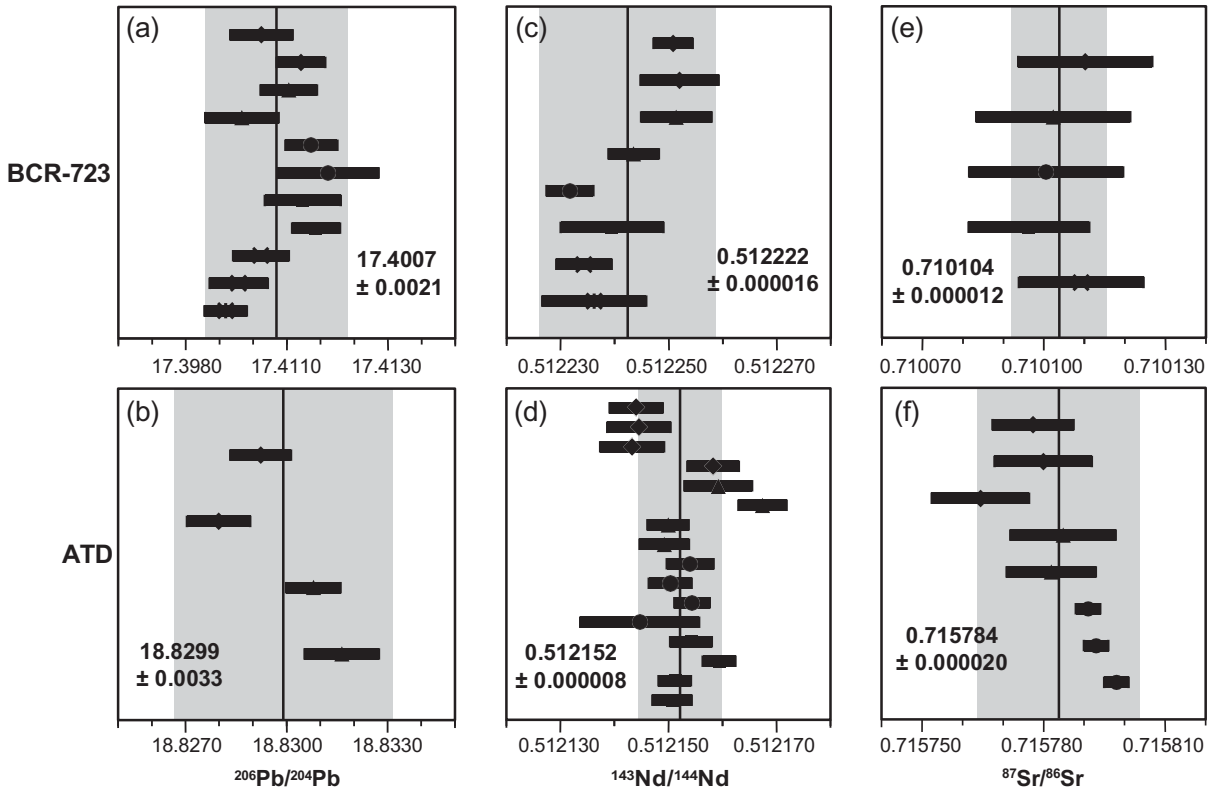

Figure 5. Compilation of $^{206}Pb/^{204}Pb$, $^{143}Nd/^{144}Nd$, $^{87}Sr/^{86}Sr$ for ATD and BCR-723 dust reference materials. Each symbol corresponds to a single duplicate and its associated replicates with their respective expanded uncertainties (k = 2). Vertical bars and their respective shaded area correspond to the mean values from duplicate measurements and the expanded uncertainty (k = 2) (values in bold), respectively.

For Zn and Cu isotopic compositions in AGV-2 (Tables 6 and 7), the expanded uncertainty (k = 2) for all duplicates was ≤ 0.04‰. The uncertainty for Fe isotopes on replicates (n = 3 min) was ≤ 0.06‰, while the expanded uncertainty (k = 2) on three duplicates was ≤ 0.04‰. Results for $\delta^{66}Zn_{JMC\ Lyon}$ for AGV-2 showed values of +0.27 ± 0.08‰ (k = 2), which corresponds to the weighted mean of +0.28 ± 0.04 (k = 2) from the literature (Figure 4a). The $\delta^{65}Cu_{NIST976}$ results raise a question, as our two duplicates exhibited quite different values at 0.13 ± 0.03‰ (k = 2), while the other was -0.05 ± 0.02‰ (k = 2). Both duplicates are out of expanded uncertainty (k = 2) range but fall well within the global weighted mean value of + 0.05 ± 0.10‰ (k = 2) (Figure 4b). Analytical conditions were equally good for both $\delta^{65}Cu_{NIST976}$ duplicates and are unlikely to explain such a difference. One reason might be a 'nugget effect' as Cu can be highly concentrated in some minerals that can strongly affect the bulk isotopic signature if the sample powder is not homogeneous enough. Concerning Fe isotopes, data in the literature display slight variation for AGV-2 with a weighted mean of +0.101 ± 0.009‰ (k = 2); our value fits in that range with a $\delta^{56}Fe_{IRMM014}$ = +0.120 ± 0.012‰ (k = 2) (Figure 4c).

Regarding G-2, the mean measured $\delta^{66}Zn_{JMC\ Lyon}$ of +0.30 ± 0.05‰ (k = 2) is in agreement with the weighted mean of +0.36 ± 0.09‰ (k = 2) compiled from the literature (Figure 4d). For Cu isotopes in G-2, to our knowledge, only Dong *et al.* (2013) proposed a value for $\delta^{65}Cu_{NIST976}$ of +0.27 ± 0.09‰ (2s), which is in line with our results of +0.29 ± 0.04‰ (k = 2) (Figure 4e). Finally, our mean G-2 value for $\delta^{56}Fe_{IRMM014}$ is + 0.166 ± 0.036‰ (k = 2, over three duplicates), which is 0.05‰ away from the literature weighted mean of + 0.115 ± 0.039‰ (k = 2) (Figure 4f), but still within the expanded uncertainty (k = 2) range.

ATD and BCR-723: The Pb, Nd, Sr, Zn, Cu and Fe isotopic compositions for the two dust reference materials – ATD and BCR-723 – were determined for the first time (Tables 3–8). For radiogenic isotopes, the following results are

reported for ATD and BCR-723, respectively, $^{206}Pb/^{204}Pb$ of 18.8299 ± 0.0033 (k = 2), 17.4007 ± 0.0021 (k = 2); $^{143}Nd/^{144}Nd$ of 0.512152 ± 0.000008 (k = 2), 0.512220 ± 0.000016 (k = 2) and $^{87}Sr/^{86}Sr$ of 0.715784 ± 0.000020 (k = 2), 0.710104 ± 0.000012 (k = 2) (Figure 5). For the non-traditional stable isotopes, the following values were obtained: $\delta^{66}Zn_{JMC\ Lyon}$ = +0.18 ± 0.04‰ (k = 2), +0.13 ± 0.06‰ (k = 2); $\delta^{65}Cu_{NIST976}$ = +0.34 ± 0.07‰ (k = 2), -0.16 ± 0.01‰ (k = 2) and $\delta^{56}Fe_{IRMM014}$ = -0.057 ± 0.049‰ (k = 2), +0.064 ± 0.039‰ (k = 2), respectively, for ATD and BCR-723. The Zn isotopic data obtained for BCR-723 (Figure 4g) are comparable to those of Dong *et al.* (2017), that is, +0.19 ± 0.06‰ (2s). On the other hand, the $\delta^{65}Cu_{NIST976}$ value of -0.16 ± 0.01‰ (k = 2) for BCR-723 falls outside the uncertainty of the value obtained by Dong *et al.* (2017) (-0.32 ± 0.13‰ (2s)) (Figure 4h). This discrepancy would require a better constraint of the $\delta^{65}Cu_{NIST976}$ value in BCR-723. Overall, the expanded uncertainty (k = 2) values of dust reference materials are similar or even better than for rock reference materials (Tables 3–8) indicating a good homogeneity in the samples.

Conclusions

To ensure high-quality isotopic measurements of atmospheric dust material, we propose a chromatographic method able to isolate six elements (Pb, Nd, Sr, Zn, Cu and Fe) from a single, typically low-mass sample. The multi-column scheme guarantees an adequate analyte recovery despite the matrix variability of dust samples, while maintaining low procedural blanks. The present study shows that classical rock reference materials (i.e., BHVO-2) are not adequate to represent dust materials to establish chromatography protocols, which emphasises the need for reference materials dedicated to dust samples. To date, there has been a lack of fully characterised dust reference materials. In this study, we fill this gap by providing the first isotopic characterisation of ATD and BCR-723, which represent two dust end-members (from mostly natural to heavily polluted road dust) with contrasting organic matter contents, element mass fractions and isotopic signatures, allowing for a large panel of applications. In the future, the widespread use of inter-calibrated dust reference materials, together with larger isotopic data sets, will improve the characterisation of local versus distal and natural versus anthropogenic dust sources. The combination of the six isotopic systems will provide a real improvement in our understanding of dust production, transport pathways, mixing processes, cloud processes and more globally on climatic impact relationships.

Acknowledgements

This work was supported by the Fonds de la recherche scientifique (FRS-FNRS) 'Grand Equipement – Infrastructure' n°. 2.5016.12 and the Belgian Science Policy (Belspo) [BR/175/A2/CHASE]. SB was supported by the FRS-FNRS PDR T.1012.14. We warmly thank William M. Landing and Peter L. Morton from Florida State University (USA) for providing us with the ATD dust. We also thank Johan Yans, Augustin Dekoninck and Miche'le Verhaert from Universite' de Namur (Belgium) for the Saharan dust precursor samples and Jacqueline Vander Auwera from Universite' de Liège (Belgium) for the dust precursor from Patagonia. Dr Christophe Que'tel and four anonymous reviewers are thanked for their relevant comments, which helped to improve the quality of this manuscript.

Conflict of interest

The authors declare no conflict of interest.

References

Aarons S.M., Aciego S.M. and Gleason J.D. (2013) Variable Hf Sr Nd radiogenic isotopic compositions in a Saharan dust storm over the Atlantic: Implications for dust flux to oceans, ice sheets and the terrestrial biosphere. Chemical Geology, 349–350, 18–26.

Arau'jo D.F., Boaventura G.R., Viers J., Mulholland D.S., Weiss D., Arau'jo D., Lima B., Ruiz I., Machado W., Babinskif M. and Dantasa E. (2017) Ion exchange chromatography and mass bias correction for accurate and precise Zn isotope ratio measurements in environmental reference materials by MC-ICP-MS. Journal of the Brazilian Chemical Society, 28, 225–235.

Archer C., Andersen M.B., Cloquet C., Conway T.M., Dong S., Ellwood M., Moore R., Nelson D.J., Rehka€mper M., Rouxel O., Samanta M., Shin K., Sohrin Y., Takanoh S. and Wasylenkii L. (2017) Inter-calibration of a proposed new primary reference standard AA-ETH Zn for zinc isotopic analysis. Journal of Analytical Atomic Spectrometry, 32, 415–419.

Barling J. and Weis D. (2008) Influence of non-spectral matrix effects onvv the accuracy of Pb isotope ratio measurement by MC-ICP-MS: Implications for the external normalization method of instrumental mass bias correction. Journal of Analytical Atomic Spectrometry, 23, 1017–1025.

references

Basile I., Grousset F.E., Revel M., Petit J.R., Biscaye P.E. and Barkov N.I. (1997)
Patagonian origin of glacial dust deposited in East Antarctica (Vostok and Dome C) during glacial stages 2, 4 and 6. Earth and Planetary Science Letters, 146, 573–589.

Beard B.L., Johnson C.M., Skulan J.L., Nealson K.H., Cox L. and Sun H. (2003)
Application of Fe isotopes to tracing the geochemical and biological cycling of Fe. Chemical Geology, 195, 87–117.

Blichert-Toft J., Chauvel C. and Albare'de F. (1997)
Separation of Hf and Lu for high-precision isotope analysis of rock samples by magnetic sector-multiple collector ICP-MS. Contributions to Mineralogy and Petrology, 127, 248–260.

Chapman J.B., Weiss D.J., Shan Y. and Lemburger M. (2009)
Iron isotope fractionation during leaching of granite and basalt by hydrochloric and oxalic acids. Geochimica et Cosmochimica Acta, 73, 1312–1324.

Chauvel C. and Blichert-Toft J. (2001)
A hafnium isotope and trace element perspective on melting of the depleted mantle. Earth and Planetary Science Letters, 190, 137–151.

Chen B., Stein A.F., Maldonado P.G., Sanchez de la Campa A.M., Gonzalez-Castanedo Y., Castell N. and de la Rosa J.D. (2013)
Size distribution and concentrations of heavy metals in atmospheric aerosols originating from industrial emissions as predicted by the HYSPLIT model. Atmospheric Environment, 71, 234–244.

Chen S., Liu Y., Hu J., Zhang Z., Hou Z., Huang F. and Yu H. (2016)
Zinc isotopic compositions of NIST SRM 683 and whole-rock reference materials. Geostandards and Geoanalytical Research, 40, 417–432.

Claquin T., Schulz M. and Balkanski Y.J. (1999)
Modeling the mineralogy of atmospheric dust sources. Journal of Geophysical Research: Atmospheres, 104, 22243–22256.

Cloquet C., Carignan J., Lehmann M.F. and Vanhaecke F. (2008)
Variation in the isotopic composition of zinc in the natural environment and the use of zinc isotopes in biogeosciences: A review. Analytical and Bioanalytical Chemistry, 390, 451–463.

Cloquet C., Carignan J. and Libourel G. (2006)
Isotopic composition of Zn and Pb atmospheric depositions in an urban/periurban area of northeastern France. Environmental Science and Technology, 40, 6594–6600.

Craddock P.R. and Dauphas N. (2011)
Iron isotopic compositions of geological reference materials and chondrites. Geostandards and Geoanalytical Research, 35, 101–123.

Dauphas N., van Zuilen M., Wadhwa M., Davis A.M., Marty B. and Janney P.E. (2004)
Clues from Fe isotope variations on the origin of early Archean BIFs from Greenland. Science, 306, 2077–2080.

Dauphas N., Pourmand A. and Teng F.-Z. (2009)
Routine isotopic analysis of iron by HR-MC-ICPMS: How precise and how accurate? Chemical Geology, 267, 175–184.

de Jong J., Schoemann V., Tison J.-L., Becquevort S., Masson F., Lannuzel D., Petit J., Chou L., Weis D. and Mattielli N. (2007)
Precise measurement of Fe isotopes in marine samples by multi-collector inductively coupled plasma mass spectrometry (MC-ICP-MS). Analytica Chimica Acta, 589, 105–119.

Delmonte B., Andersson P.S., Scho€berg H., Hansson M., Petit J.R., Delmas R., Gaiero D.M., Maggi V. and Frezzotti M. (2010)
Geographic provenance of aeolian dust in East Antarctica during Pleistocene glaciations: Preliminary results from Talos Dome and comparison with East Antarctic and new Andean ice core data. Quaternary Science, Reviews, 29, 256–264.

Dideriksen K., Baker J.A. and Stipp S.L.S. (2006)
Iron isotopes in natural carbonate minerals determined by MC-ICP-MS with a ^{58}Fe–^{54}Fe double spike. Geochimica et Cosmochimica Acta, 70, 118–132.

Dong S., Ochoa G.R., Harrison R.M., Green D., North R., Fowler G. and Weiss D. (2017)
Isotopic signatures suggest important contributions from recycled gasoline, road dust and non-exhaust traffic sources for copper, zinc and lead in PM 10 in London, United Kingdom. Atmospheric Environment, 165, 88–98.

Dong S., Weiss D.J., Strekopytov S., Kreissig K., Sun Y., Baker A.R. and Formenti P. (2013)
Stable isotope ratio measurements of Cu and Zn in mineral dust (bulk and size fractions) from the Taklimakan Desert and the Sahel and in aerosols from the eastern tropical North Atlantic Ocean. Talanta, 114, 103–109.

Ehrlich S., Gavrieli I., Dor L.-B. and Halicz L. (2001)
Direct high-precision measurements of the $^{87}Sr/^{86}Sr$ isotope ratio in natural water, carbonates and related materials by multiple collector inductively coupled plasma-mass spectrometry (MC-ICP-MS). Journal of Analytical Atomic Spectrometry, 16, 1389–1392.

Fehr M.A., Andersson P.S., H@lenius U. and Mo€rth C.-M. (2008)
Iron isotope variations in Holocene sediments of the Gotland Deep, Baltic Sea. Geochimica et Cosmochimica Acta, 72, 807–826.

Flament P., Mattielli N., Aimoz L., Choe€l M., Deboudt K., de Jong J., Rimetz-Planchon J. and Weis D. (2008)
Iron isotopic fractionation in industrial emissions and urban aerosols. Chemosphere, 73, 1793–1798.

Formenti P., Caquineau S., Desboeufs K., Klaver A., Chevaillier S., Journet E. and Rajot J.L. (2014)
Mapping the physico-chemical properties of mineral dust in western Africa: Mineralogical composition. Atmospheric Chemistry and Physics Discussions, 14, 10241–10310.

references

Fourny A., Weis D. and Scoates J.S. (2016)
Comprehensive Pb-Sr-Nd-Hf isotopic, trace element, and mineralogical characterization of mafic to ultramafic rock reference materials: Mafic-ultramafic reference materials. Geochemistry, Geophysics, Geosystems, 17, 739–773.

Galer S.J.G. and Abouchami W. (1998)
Practical application of lead triple spiking for correction of instrumental mass discrimination. Mineral Magazine, A62, 491–492.

Gar_con M., Sauze'at L., Carlson R.W., Shirey S.B., Simon M., Balter V. and Boyet M. (2017)
Nitrile, latex, neoprene and vinyl gloves: A primary source of contamination for trace element and Zn isotopic analyses in geological and biological samples. Geostandards and Geoanalytical Research, 41, 367–380.

Gioia S., Weiss D., Coles B., Arnold T. and Babinski M. (2008)
Accurate and precise zinc isotope ratio measurements in urban aerosols. Analytical Chemistry, 80, 9776–9780.

Grousset F.E. and Biscaye P.E. (2005)
Tracing dust sources and transport patterns using Sr, Nd and Pb isotopes. Chemical Geology, 222, 149–167.

Hamilton P.J., O'Nions R.K., Bridgwater D. and Nutman A. (1983)
Sm-Nd studies of Archaean metasediments and metavolcanics from West Greenland and their implications for the Earth's early history. Earth and Planetary Science Letters, 62, 263–272.

He Y., Ke S., Teng F.-Z., Wang T., Wu H., Lu Y. and Li S. (2015)
High-precision iron isotope analysis of geological reference materials by high-resolution MC-ICP-MS. Geostandards and Geoanalytical Research, 39, 341–356.

Hoefs J. (2004)
Stable isotope geochemistry. Springer (Berlin, Heidelberg), 286pp.

Hoffer E.M., Kothny E.L. and Appel B.R. (1979)
Simple method for microgram amounts of sulfate in atmospheric particulates. Atmospheric Environment, 13, 303–306.

John S.G., Park J.G., Zhang Z. and Boyle E.A. (2007)
The isotopic composition of some common forms of anthropogenic zinc. Chemical Geology, 245, 61–69.

John S.G. and Adkins J.F. (2010)
Analysis of dissolved iron isotopes in seawater. Marine Chemistry, 119, 65–76.

Jweda J., Bolge L., Class C. and Goldstein S.L. (2016)
High precision Sr-Nd-Hf-Pb isotopic compositions of USGS reference material BCR-2. Geostandards and Geoanalytical Research, 40, 101–115.

Koma'rek M., Ettler V., Chrastn'y V. and Mihaljevivc M. (2008)
Lead isotopes in environmental sciences: A review. Environment International, 34, 562–577.

Kraus K.A. and Moore G.E. (1953)
Anion exchange studies. VI.1,2 The divalent transition elements manganese to zinc in hydrochloric acid. Journal of the American Chemical Society, 75, 1460–1462.

Kraus K.A. and Nelson F. (1958)
Metal separations by anion exchange. In: Materials A.S.F.T. (ed.), Ion exchange and chromatography in analytical chemistry, ASTM Special Technical Publication, 195. ASTM International (Atlantic City), 27–59.

Le Roux G., Fagel N., De Vleeschouwer F., Krachler M., Debaille V., Stille P., Matielli N., van der Knaap W.O., van Leeuwen J. and Shotyk W. (2012)
Volcano- and climate-driven changes in atmospheric dust sources and fluxes since the Late Glacial in Central Europe. Geology, 40, 335–338.

Le Roux G. and De Vleeschouwer F. (2010)
Preparation of peat samples for inorganic geochemistry used as palaeoenvironmental proxies. Mires and Peat, 7, 1.

Liu S.-A., Li D., Li S., Teng F.-Z., Ke S., He Y. and Lu Y. (2014)
High-precision copper and iron isotope analysis of igneous rock standards by MC-ICP-MS. Journal of Analytical Atomic Spectrometry, 29, 122–133.

Long C.M., Nascarella M.A. and Valberg P.A. (2013)
Carbon black vs. black carbon and other airborne materials containing elemental carbon: Physical and chemical distinctions. Environmental Pollution, 181, 271–286.

Mahowald N., Albani S., Kok J.F., Engelstaeder S., Scanza R., Ward D.S. and Flanner M.G. (2014)
The size distribution of desert dust aerosols and its impact on the Earth system. Aeolian Research, 15, 53–71.

Mare'chal C.N., Te'louk P. and Albare'de F. (1999)
Precise analysis of copper and zinc isotopic compositions by plasma-source mass spectrometry. Chemical Geology, 156, 251–273.

Martin J.H. (1990)
Glacial-interglacial CO_2 change: The iron hypothesis. Paleoceanography, 5, 1–13.

Mason T.F.D., Weiss D.J., Horstwood M., Parrish R.R., Russell S.S., Mullane E. and Coles B.J. (2004)
High-precision Cu and Zn isotope analysis by plasma source mass spectrometry. Journal of Analytical Atomic Spectrometry, 19, 218.

Mattielli N., Petit J.C.J., Deboudt K., Flament P., Perdrix E., Taillez A., Rimetz-Planchon J. and Weis D. (2009)
Zn isotope study of atmospheric emissions and dry depositions within a 5 km radius of a Pb–Zn refinery. Atmospheric Environment, 43, 1265–1272.

references

McTainsh G. and Strong C. (2007)
The role of aeolian dust in ecosystems. Geomorphology, 89, 39–54.

Millet M.-A., Baker J.A. and Payne C.E. (2012)
Ultra-precise stable Fe isotope measurements by high resolution multiple-collector inductively coupled plasma mass spectrometry with a ^{57}Fe–^{58}Fe double spike. Chemical Geology, 304–305, 18–25.

Moeller K., Schoenberg R., Pedersen R.-B., Weiss D. and Dong S. (2012)
Calibration of the new certified reference materials ERM-AE633 and ERM-AE647 for copper and IRMM-3702 for zinc isotope amount ratio determinations. Geostandards and Geoanalytical Research, 36, 177–199.

Moynier F., Beck P., Yin Q.-Z., Ferroir T., Barrat J.-A., Paniello R., Te'louk P. and Gillet P. (2010)
Volatilization induced by impacts recorded in Zn isotope composition of ureilites. Chemical Geology, 276, 374–379.

Ochoa Gonzalez R., Strekopytov S., Amato F., Querol X., Reche C. and Weiss D. (2016)
New insights from zinc and copper isotopic compositions into the sources of atmospheric particulate matter from two major European cities. Environmental Science and Technology, 50, 9816–9824.

Paniello R.C., Day J.M.D. and Moynier F. (2012a)
Zinc isotopic evidence for the origin of the Moon. Nature, 490, 376–379.

Paniello R.C., Moynier F., Beck P., Barrat J.-A., Podosek F.A. and Pichat S. (2012b)
Zinc isotopes in HEDs: Clues to the formation of 4-Vesta, and the unique composition of Pecora Escarpment 82502. Geochimica et Cosmochimica Acta, 86, 76–87.

Perlwitz J., Tegen I. and Miller R.L. (2001)
Interactive soil dust aerosol model in the GISS GCM: 1. Sensitivity of the soil dust cycle to radiative properties of soil dust aerosols. Journal of Geophysical Research: Atmospheres, 106, 18167–18192.

Petit J.C., De Jong J., Chou L. and Mattielli N. (2008)
Development of Cu and Zn isotope MC-ICP-MS measurements: Application to suspended particulate matter and sediments from the Scheldt Estuary. Geostandards and Geoanalytical Research, 32, 149–166.

Petit J.C.J., Taillez A. and Mattielli N. (2013)
A case study of spectral and non-spectral interferences on copper isotope measurements by multi-collector ICP-MS (wet plasma). Geostandards and Geoanalytical Research, 37, 319–335.

Pin C., Briot D., Bassin C. and Poitrasson F. (1994)
Concomitant separation of strontium and samarium-neodymium for isotopic analysis in silicate samples, based on specific extraction chromatography. Analytica Chimica Acta, 298, 209–217.

Pin C., Gannoun A. and Dupont A. (2014)
Rapid, simultaneous separation of Sr, Pb, and Nd by extraction chromatography prior to isotope ratios determination by TIMS and MC-ICP-MS. Journal of Analytical Atomic Spectrometry, 29, 1858–1870.

Ponzevera E., Que'tel C.R., Berglund M., Taylor P.D.P., Evans P., Loss R.D. and Fortunato G. (2006)
Mass discrimination during MC-ICP-MS isotopic ratio measurements: Investigation by means of synthetic isotopic mixtures (IRMM-007 series) and application to the calibration of natural-like zinc materials (including IRMM-3702 and IRMM-651). Journal of the American Society for Mass Spectrometry, 17, 1413–1427.

Retzmann A., Zimmermann T., Pro€frock D., Prohaska T. and Irrgeher J. (2017)
A fully automated simultaneous single-stage separation of Sr, Pb, and Nd using DGA Resin for the isotopic analysis of marine sediments. Analytical and Bioanalytical Chemistry, 409, 5463–5480.

Richard P., Shimizu N. and Alle'gre C.J. (1976)
$^{143}Nd/^{146}Nd$, a natural tracer: An application to oceanic basalts. Earth and Planetary Science Letters, 31, 269–278.

Rizzolo J.A., Barbosa C., Borillo G., Godoi A., Souza R., Andreoli R., Manzi A., Sa' M., Alves E., Po€hlker C., Angelis I., Ditas F., Saturno J., Moran-Zuloaga D., Rizzo L., Rosa'rio N., Pauliquevis T., Santos R., Yamamoto C., Andreae M., Artaxo P., Taylor F. and Godoi R. (2017)
Soluble iron nutrients in Saharan dust over the central Amazon rainforest. Atmospheric Chemistry and Physics, 17, 2673–2687.

Roe J.E., Anbar A.D. and Barling J. (2003)
Nonbiological fractionation of Fe isotopes: Evidence of an equilibrium isotope effect. Chemical Geology, 195, 69–85.

Rousseau D., Chauvel C., Sima A., Hatte' C., Lagroix F., Antoine P., Balkanski Y., Fuchs M., Mellett C., Kageyama M., Ramstein G. and Lang A. (2014)
European glacial dust deposits: Geochemical constraints on atmospheric dust cycle modeling: European glacial dust deposits. Geophysical Research Letters, 41, 7666–7674.

Rosman K.J.R. and Taylor P.D.P. (1998)
Isotopic composition of the elements 1997 (Technical report). Pure and Applied Chemistry, 70, 217–235.

Saito N. (1984)
Selected data on ion exchange separations in radioanalytical chemistry. Pure and Applied Chemistry, 56, 523–539.

Savage P.S., Moynier F., Chen H., Shofner G., Siebert J., Badro J. and Puchtel I.S. (2015)
Copper isotope evidence for large-scale sulphide fractionation during Earth's differentiation. Geochemical Perspectives Letters, 1, 53–64.

references

Scheuvens D., Schu€tz L., Kandler K., Ebert M. and Weinbruch S. (2013)
Bulk composition of northern African dust and its source sediments – A compilation. Earth-Science Reviews, 116, 170–194.

Shelley R.U., Morton P.L. and Landing W.M. (2015)
Elemental ratios and enrichment factors in aerosols from the US-GEOTRACES North Atlantic transects. Deep Sea Research Part II: Topical Studies in Oceanography, 116, 262–272.

Shiel A.E., Barling J., Orians K.J. and Weis D. (2009)
Matrix effects on the multi-collector inductively coupled plasma-mass spectrometric analysis of high-precision cadmium and zinc isotope ratios. Analytica Chimica Acta, 633, 29–37.

Sossi P.A., Halverson G.P., Nebel O. and Eggins S.M. (2015)
Combined separation of Cu, Fe and Zn from rock matrices and improved analytical protocols for stable isotope determination. Geostandards and Geoanalytical Research, 39, 129–149.

Souto-Oliveira C.E., Babinski M., Arau'jo D.F. and Andrade M.F. (2018)
Multi-isotopic fingerprints (Pb, Zn, Cu) applied for urban aerosol source apportionment and discrimination. Science of the Total Environment, 626, 1350–1366.

Wang K., Moynier F., Dauphas N., Barrat J.-A., Craddock P. and Sio C.K. (2012)
Iron isotope fractionation in planetary crusts. Geochimica et Cosmochimica Acta, 89, 31–45.

Wang Z., Pan X., Uno I., Chen X., Yamamoto S., Zheng H., Li J. and Wang Z. (2018)
Importance of mineral dust and anthropogenic pollutants mixing during a long-lasting high PM event over East Asia. Environmental Pollution, 234, 368–378.

Weinstein C., Moynier F., Wang K., Paniello R., Foriel J., Catalano J. and Pichat S. (2011)
Isotopic fractionation of Cu in plants. Chemical Geology, 286, 266–271.

Weis D., Kieffer B., Maerschalk C., Barling J., de Jong J., Williams G., Hanano D., Pretorius W., Mattielli N., Scoates J., Goolaerts A., Friedman R. and Mahoney J. (2006)
High-precision isotopic characterization of USGS reference materials by TIMS and MC-ICP-MS: Isotopic study of USGS reference materials. Geochemistry, Geophysics, Geosystems, 7(8).

Weiss D.J., Rehka€mper M., Schoenberg R., McLaughlin M., Kirby J., Campbell P., Arnold T., Chapman J., Peeland K. and Gioia S. (2008)
Application of non-traditional stable-isotope systems to the study of sources and fate of metals in the environment. Environmental Science and Technology, 42, 655–664.

Wiederhold J.G. (2015)
Metal stable isotope signatures as tracers in environmental geochemistry. Environmental Science and Technology, 49, 2606–2624.

Wientjes I.G.M., Van de Wal R.S.W., Reichart G.J., Sluijs A. and Oerlemans J. (2011)
Dust from the dark region in the western ablation zone of the Greenland ice sheet. The Cryosphere, 5, 589–601.